

# A Review of Electrocatalytic Reduction of Dinitrogen to Ammonia under Ambient Conditions

Xiaoyang Cui, Cheng Tang, and Qiang Zhang\*

The production of ammonia ( $\text{NH}_3$ ) from molecular dinitrogen ( $\text{N}_2$ ) under mild conditions is one of the most attractive topics in the field of chemistry. Electrochemical reduction of  $\text{N}_2$  is promising for achieving clean and sustainable  $\text{NH}_3$  production with lower energy consumption using renewable energy sources. To date, emerging electrocatalysts for the electrochemical reduction of  $\text{N}_2$  to  $\text{NH}_3$  at room temperature and atmospheric pressure remain largely underexplored. The major challenge is to achieve both high catalytic activity and high selectivity. Here, the recent progress on the electrochemical nitrogen reduction reaction (NRR) at ambient temperature and pressure from both theoretical and experimental aspects is summarized, aiming at extracting instructive perceptions for future NRR research activities. The prevailing theories and mechanisms for NRR as well as computational screening of promising materials are presented. State-of-the-art heterogeneous electrocatalysts as well as rational design of the whole electrochemical systems for NRR are involved. Importantly, promising strategies to enhance the activity, selectivity, efficiency, and stability of electrocatalysts toward NRR are proposed. Moreover, ammonia determination methods are compared and problems relating to possible ammonia contamination of the system are mentioned so as to shed fresh light on possible standard protocols for NRR measurements.

## 1. Introduction

With the ever increasing global population, the impending depletion of fossil fuels and pressing worldwide environmental concerns, the search for sustainable, renewable, and eco-friendly energy pathways is strongly demanded to secure our energy future. As an essential part of sustainable energy systems, electrochemical energy conversion devices enable the production of valuable chemicals including hydrogen, hydrocarbons, oxygenates, and ammonia from the abundant feedstock of water, carbon dioxide, oxygen, and nitrogen on earth. In these energy conversion devices, electrocatalysts play an indispensable role, facilitating the efficiency and selectivity of the chemical

reactions involved.<sup>[1]</sup> In recent years, tremendous progress has been achieved in the field of heterogeneous electrocatalysis, with rapid development of multifarious electrocatalysts toward oxygen reduction reaction (ORR), oxygen evolution reaction (OER), hydrogen evolution reaction (HER), and carbon dioxide reduction reaction ( $\text{CO}_2\text{RR}$ ). However, electrocatalysts for the reduction of dinitrogen ( $\text{N}_2$ ) to ammonia ( $\text{NH}_3$ ) at room temperature and atmospheric pressure remain largely underexplored, despite the fact that investigations on catalysts and reaction systems for artificial nitrogen fixation have been continued for more than 100 years.<sup>[2–4]</sup>

Ammonia is primarily used for producing fertilizers to sustain the world's population.<sup>[5]</sup> It also serves as a green energy carrier and a potential transportation fuel.<sup>[6]</sup> Currently, ammonia synthesis is dominated by the industrial Haber–Bosch process using heterogeneous iron-based catalysts at high temperature (300–500 °C) and high pressure (150–300 atm),<sup>[7]</sup> accounting for more

than 1% of the world's energy supply and generating more than 300 million metric tons of fossil fuel-derived  $\text{CO}_2$  annually.<sup>[8,9]</sup> Hence, it is desirable to develop alternative processes that have the potential to overcome the limitations of the Haber–Bosch process including harsh conditions, complex plant infrastructure, centralized distribution, high energy consumption, and negative environmental impacts.

In nature, biological  $\text{N}_2$  fixation occurs under mild conditions via nitrogenase enzymes that contain FeMo, FeV, or FeFe cofactor as catalytic active sites.<sup>[10,11]</sup> Developed man-made catalysts are therefore stimulated to reduce  $\text{N}_2$  upon the addition of protons and electrons, which is similar to the nitrogenase catalytic process. Transition metal–dinitrogen complexes such as the molybdenum–, iron–, and cobalt–dinitrogen complexes have been proposed as homogeneous catalysts for the reduction of  $\text{N}_2$  into  $\text{NH}_3$  under ambient conditions;<sup>[12]</sup> however, the stability and recycling issues are challenging.<sup>[13]</sup>

On the other hand, electrochemical and photochemical reduction processes using heterogeneous catalysts benefit from clean and renewable energy sources and are promising for achieving  $\text{NH}_3$  production directly from  $\text{N}_2$  and water.<sup>[14]</sup> The electrochemical reduction of  $\text{N}_2$  to  $\text{NH}_3$  can be more efficient than the photochemical counterpart. This is because not all of the photons in the photochemical reduction process can

Dr. X. Y. Cui, C. Tang, Prof. Q. Zhang  
Beijing Key Laboratory of Green Chemical Reaction Engineering and Technology  
Department of Chemical Engineering  
Tsinghua University  
Beijing 100084, China  
E-mail: zhang-qiang@mails.tsinghua.edu.cn

 The ORCID identification number(s) for the author(s) of this article can be found under <https://doi.org/10.1002/aenm.201800369>.

DOI: 10.1002/aenm.201800369

be utilized due to multiple wavelengths and fast charge carrier recombination. In contrast, a fixed potential can be used in the electrochemical reduction process to generate the desired product.<sup>[15]</sup> Compared to the conventional Haber–Bosch process, the electrochemical reduction process under mild conditions renders the feasibility to reduce the energy input, cut down the carbon footprint, simplify the reactor design, and ease the complexity of ammonia production plants.

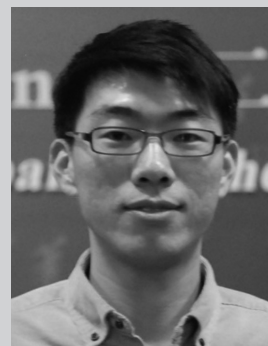
In theory, electrochemical reduction of N<sub>2</sub> to NH<sub>3</sub> on a heterogeneous surface is possible at room temperature and atmospheric pressure as long as a sufficient voltage is applied.<sup>[16]</sup> However, in practice there is a lack of catalysts available that can produce NH<sub>3</sub> in significant yields and with high Faradaic efficiencies (FEs). The grand challenge is that heterogeneous catalyst surfaces that are active for the reduction of N<sub>2</sub> to NH<sub>3</sub> in the presence of water are also highly active for the reduction of water molecules to hydrogen gas. Most of the protons and electrons in the system go toward the hydrogen evolution reaction (HER) rather than the nitrogen reduction reaction (NRR), resulting in a severe selectivity issue.<sup>[17]</sup> In recent years, there is a blossoming interest in the field of electrochemical reduction of N<sub>2</sub> to NH<sub>3</sub> under mild conditions. Prolific achievements have been made, yet major obstacles remain for improving both catalytic activity and selectivity.<sup>[18–21]</sup>

In this review, we present recent progress in electrochemical reduction of N<sub>2</sub> to NH<sub>3</sub> under ambient temperature and pressure from both theoretical and experimental perspectives, aiming at extracting instructive perceptions for future NRR research activities. Herein we begin by introducing the prevailing mechanisms for the reduction of N<sub>2</sub> to NH<sub>3</sub> at a heterogeneous surface under ambient conditions. The advances and bottlenecks in electrocatalytic NRR are reviewed from computational investigations. Furthermore, we briefly review the pioneering classical electrochemical literatures in this area, and then move on to state-of-the-art electrocatalysts and devices capable of electrochemical reduction of N<sub>2</sub> to NH<sub>3</sub> under ambient conditions. In addition, different methods for the determination of ammonia are compared to promote possible standard protocols for NRR testing.

Finally, we summarize the existing challenges in electrocatalytic dinitrogen reduction and propose promising strategies for improving the activity, selectivity, efficiency, and stability of heterogeneous electrocatalysts toward NRR (**Figure 1**). In this context, the intrinsic activity of an individual active site is influenced by the electronic structure, whereas the apparent activity (such as the turnover and yield) is impacted by the material structure and morphology (crystal facets, size, shape, dimension, etc.) and associates with the number of and the diffusion to the active sites. Hence, on one hand, cationic/anionic regulation, heteroatom doping, and defect/strain engineering can change the electronic structure to achieve high intrinsic activity. On the other hand, the surface area, pore structure, along with hybridization of active sites and supports that ensure adequate exposure and utilization of active sites can boost the apparent activity.<sup>[22]</sup> Importantly, the selectivity governs the purity of the desired products and directly correlates to the chemical features of the electrocatalyst surfaces. The surface adsorbing/desorbing properties can influence the activation of the N≡N triple bond and the addition of protons to the nitrogen atoms



**Xiaoyang Cui** received her PhD in 2016 in the School of Materials Science and Engineering, Tsinghua University. She is currently a postdoctoral fellow in the Department of Chemical Engineering, Tsinghua University. Her current research interest is the development of nanomaterials and electrochemical systems toward sustainable energy electrocatalysis, especially focusing on rational design of electrocatalytic systems toward nitrogen reduction reaction under ambient conditions.



**Cheng Tang** received his B.E. degree in 2013 in the Department of Chemical Engineering, Tsinghua University, and is currently pursuing his Ph.D. there. His research interests focus on nanomaterials and energy electrocatalysis, including 3D graphene materials, hierarchical hybrids, oxygen reduction/evolution, hydrogen evolution reaction, nitrogen reduction reaction, etc.



**Qiang Zhang** received his bachelor and Ph.D. degree from Tsinghua University in 2004 and 2009, respectively. After a stay as a research associate in Case Western Reserve University, USA, he joined the Fritz Haber Institute of the Max Planck Society, Germany. Now he is a full professor at Tsinghua University. His interests focus on energy materials, includes Li-S batteries, lithium metal anode, and electrocatalysis.

in order to form ammonia. Moreover, rational design of the catalyst/electrolyte interface and the electrode/catalyst interface can suppress the competing HER via controlling the proton availability and the electron transfer rate. The efficiency, in other words, the energy cost of the process, depends on the electrochemical properties of the whole system. To improve the efficiency, both mass and electron transport should be considered. For porous materials, the number of active sites that are exposed to the feed gas is limited. The mass transport issue can be mitigated by tuning the thickness of the electrocatalyst

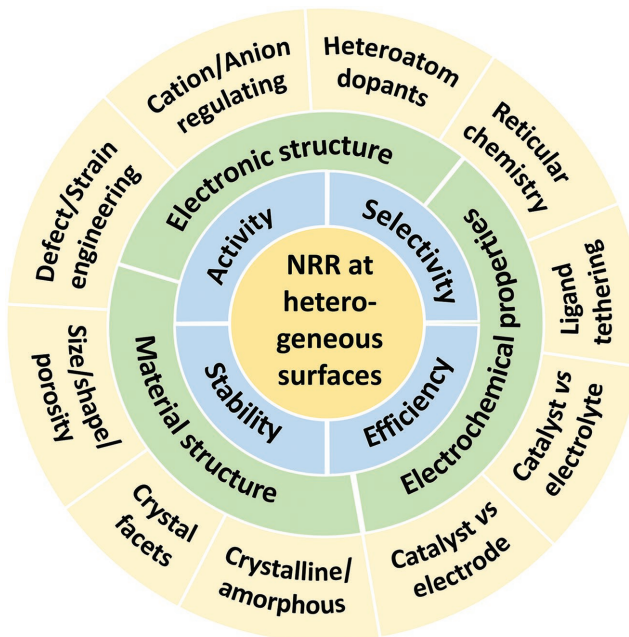


**Figure 1.** Schematic overview of strategies to enhance heterogeneous electrocatalytic conversion of  $\text{N}_2$  to  $\text{NH}_3$  at ambient conditions.

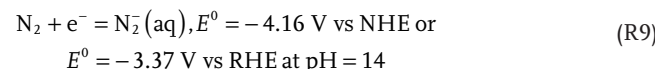
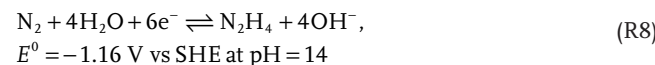
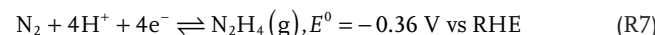
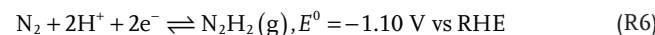
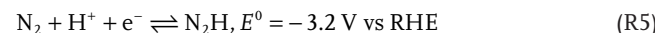
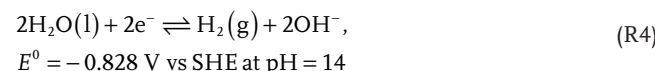
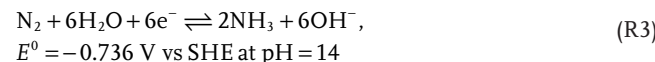
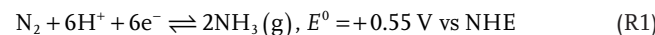
layer, whereas the electron transport issue can be solved by growing the catalysts on conductive substrates and rational design of the electrochemical reactor. The  $\text{NH}_3$  Faradaic efficiency (FE) or current efficiency (CE) is often used to roughly represent the  $\text{NH}_3$  selectivity of the electrochemical system. Additionally, the stability relates to the deactivation and decomposition of the catalysts in an electrochemical system, which can be problematic for practical application and should be taken into consideration when searching for effective electrocatalysts toward NRR.

## 2. Reaction Mechanisms of NRR

### 2.1. Thermodynamics of NRR

The inertness of the dinitrogen ( $\text{N}_2$ ) molecule is only partly due to the high bond energy ( $941 \text{ kJ mol}^{-1}$ ) of the triple bond. Considering the fact that the triple bond energy ( $962 \text{ kJ mol}^{-1}$ ) in acetylene ( $\text{C}_2\text{H}_2$ ) is higher but  $\text{C}_2\text{H}_2$  is much more reactive than  $\text{N}_2$ , the much higher first bond cleavage energy of  $\text{N}_2$  ( $410 \text{ kJ mol}^{-1}$ ) than that of  $\text{C}_2\text{H}_2$  ( $222 \text{ kJ mol}^{-1}$ ) is an apparent reason for the reactivity difference. The addition of the first H atom to  $\text{N}_2$  is endothermic ( $\Delta H^\circ = +37.6 \text{ kJ mol}^{-1}$ ), whereas the reaction to  $\text{C}_2\text{H}_2$  is exothermic ( $\Delta H^\circ = -171 \text{ kJ mol}^{-1}$ ). Consequently, direct protonation is often permitted for  $\text{C}_2\text{H}_2$ , but thermodynamically forbidden for  $\text{N}_2$ .<sup>[23]</sup> The negative electron affinity ( $-1.9 \text{ eV}$ ) and high ionization potential ( $15.8 \text{ eV}$ ) add to the resistance of  $\text{N}_2$  to Lewis acid/base. The large energy gap ( $10.82 \text{ eV}$ ) between the highest occupied molecular orbital (HOMO) and the lowest unoccupied molecular orbital (LUMO) of  $\text{N}_2$  does not favor electron transfer processes.<sup>[24,25]</sup>

The fundamental bottlenecks in the electrochemical reduction of  $\text{N}_2$  to  $\text{NH}_3$  can be understood from the thermodynamic constraints imposed by the intermediates of the reaction. The equilibrium potentials required for different NRR products with either normal hydrogen electrode (NHE), standard hydrogen electrode (SHE), or reversible hydrogen electrode (RHE) as reference can be expressed as follows:<sup>[9,26,27]</sup>



The equilibrium potentials of the electrochemical reduction of  $\text{N}_2$  to  $\text{NH}_3$  are comparable to that of the competing HER (Reaction (1) vs Reaction (2); Reaction (3) vs Reaction (4)). This is in agreement with the fact that  $\text{H}_2$  is the major side product for NRR in aqueous electrolytes. Nevertheless, the NRR is carried out via multiple proton-electron transfer reactions, and multiple intermediates are involved. The much negative redox potentials for the formation of the  $\text{N}_2\text{H}$  intermediate indicate the difficulty of initial H atom addition (Reaction (5)). A sufficiently high pH is requested for Reaction (9) to compete with Reaction (5). Moreover, adding the second H atom can be more difficult than adding the third H, resulting in larger redox potentials for the two-electron and four-electron reduction processes than the six-electron reduction processes (Reactions (6), (7), and (8)). These much negative potentials of the intermediates illustrate the thermodynamic difficulty of  $\text{N}_2$  hydrogenation.

The thermodynamic approach has revealed critical limitations of multistep catalytic reactions involving many intermediates. These intermediates have energetic relationships with each other, namely that the relative adsorption energies of the multiple intermediates correlated with each other, called the “scaling relations.”<sup>[28]</sup> Hence, the unfavorable scaling relation between the adsorption energies of two (or more) intermediates makes it difficult to reach an optimal catalyst that has

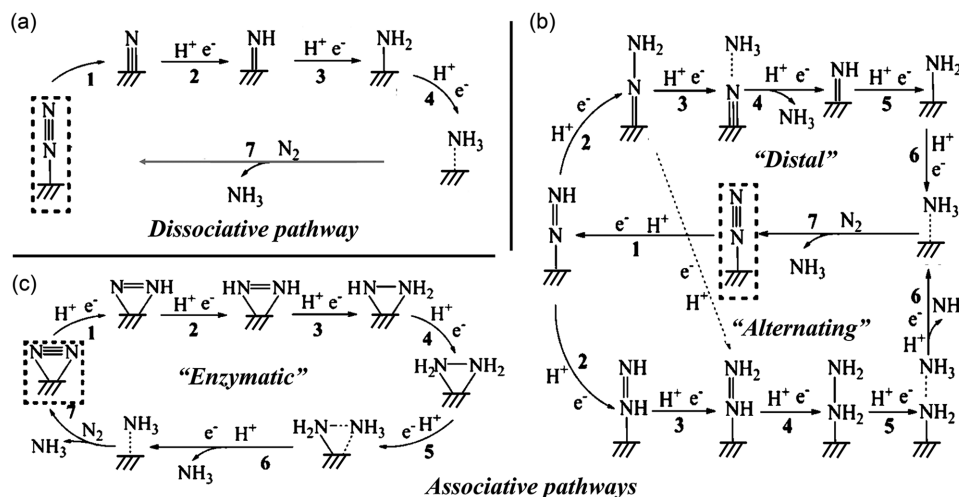


**Figure 2.** a–c) Schematic depiction of the dissociative pathway and the associative pathways (including distal, alternating, and enzymatic pathway) for catalytic conversion of  $\text{N}_2$  to  $\text{NH}_3$ . Reproduced with permission.<sup>[68]</sup> Copyright 2016, American Chemical Society.

all reaction steps being thermodynamically neutral or downhill for the overall reaction to take place. For ORR and OER, the scaling between the OOH and the OH intermediates demands a minimum overpotential for both ORR and OER of  $\approx 0.25\text{--}0.35$  V.<sup>[29,30]</sup> For NRR, the binding energies of the  $\text{NH}_2$  and  $\text{N}_2\text{H}$  intermediates are not independent, and the unfavorable scaling between them leads to a minimum overpotential of  $\approx 0.4$  V.<sup>[9]</sup> Fortunately, recent theoretical calculations have revealed that the scaling relations of NRR can be broken or circumvent with some new strategies to reduce the overpotential, which will be discussed in latter sections of this review.

Moreover, it is not clear that whether NRR prefers to follow a concerted proton–electron transfer (CPET) pathway or a sequential proton–electron transfer (SPET) pathway yet. For solid metallic electrocatalysts, the CPET pathway was often assumed; however, there is growing evidence for the significance of the SPET pathway nowadays.<sup>[31,32]</sup> Recent reports elicit that selectivity between CPET and SPET is pH dependent;<sup>[32]</sup> however, most of the computational work on NRR so far did not take the pH effect into account. In the CPET pathway, the HER is more probably to occur as  $\text{H}^+$  and  $\text{e}^-$  are transferred in a coupled hydrogen atom-like manner. In the SPET pathway,  $\text{H}^+$  tends to attack the activated nitrogen, and an electron is added to the positively charged protonated nitrogen intermediate. It has been estimated that the activation barrier for the SPET reaction is lower than the activation barrier for the CPET reaction for NRR; hence, the SPET pathway is preferred compared to the CPET pathway.<sup>[33]</sup> Still, more investigations are requested to address the selection or competition between CPET and SPET pathways in electrocatalytic NRR mechanisms over heterogeneous catalysts at ambient conditions.

## 2.2. Reaction Mechanisms of NRR

Generally speaking, the proposed mechanisms for electrochemical reduction of  $\text{N}_2$  to  $\text{NH}_3$  can be classified into 1) the

dissociative pathway and 2) the associative pathway. In the dissociative pathway, the  $\text{N}\equiv\text{N}$  triple bond is broken before the addition of H to the N atoms (Figure 2a), whereas in the associative pathway, the N–N bond is cleaved simultaneously with the release of the first molecule of  $\text{NH}_3$ . The associative pathway can be further divided into the distal pathway and the alternating pathway according to different hydrogenation sequences. In the distal pathway, the remote nitrogen atom is hydrogenated first and released as  $\text{NH}_3$ , whereas in the alternating pathway, the two N atoms are hydrogenated simultaneously (Figure 2b).<sup>[9]</sup> Notably, the enzymatic pathway, which belongs to the associative pathway, exhibits a distinctive feature of its side-on adsorption mode of N atoms (Figure 2c), instead of an end-on adsorption mode of N atoms proposed on most heterogeneous surfaces.

Recently, Abghou and Skúlason proposed that a Mars–van Krevelen (MvK) mechanism is more favorable than the routine dissociative mechanism and associative mechanism on the surface of transition metal nitrides (TMNs).<sup>[34]</sup> In the MvK mechanism for TMNs, a lattice N atom on the surface of metal nitrides is reduced to  $\text{NH}_3$  and the catalyst later regenerated with gaseous  $\text{N}_2$ , which differs from the conventional dissociative mechanism and associative mechanism. Density functional theory (DFT) calculation revealed that the dissociative mechanism is inhibitive for that the dissociation of  $\text{N}_2$  on the clean surfaces of TMNs is endothermic and the activation barriers are large. The overpotential predicted for  $\text{N}_2$  reduction and  $\text{NH}_3$  formation is smaller via MvK mechanism than that via associative mechanism.<sup>[34]</sup>

## 3. Recent Theoretical Advances in NRR

The advances of computational methods not only facilitate the exploration of efficient catalysts and trend prediction in chemical reaction rates, but also provide emerging understanding of the mechanisms and interpret experimental data with mechanistic insights and **structure–reactivity correlations**. Herein we describe recent theoretical practices on various kinds of heterogeneous surfaces based on DFT calculations for material

screening and prediction of promising catalysts for electrochemical reduction of N<sub>2</sub> to NH<sub>3</sub> at ambient conditions.

### 3.1. The Scaling Relations

In heterogeneous catalysis, the Sabatier principle has provided a qualitative framework for the optimum catalyst: catalyst that binds atoms and molecules neither too weakly to activate the reactants nor too strongly to desorb the products. If the binding is too weak, the catalyst is unable to activate the reactant; if the binding is too strong, the catalyst will be poisoned by the strongly adsorbed intermediates. This leads to a volcano-type relationship between bond strength and catalytic activity.<sup>[35]</sup> In order to quantify the bond strength, descriptions of the interaction between the surface and the chemical species involved in the reactions are highly desired. However, a heterogeneous surface can be too complex to be quantitatively modeled in their entirety because a variety of adsorbed intermediates and transition states of many different classes of elementary steps interact with the surface. Hence, linear energy relations were used to simplify the theoretical analysis and provided new insight into the underlying trends of catalytic reactions across a vast space of catalytic surfaces. The linear energy relations in question include the Brønsted–Evans–Polanyi relations which relate the transition state activation energy of elementary reactions to the thermodynamics of those reactions,<sup>[36,37]</sup> and the scaling relations which describe correlations between the adsorption energies of different adsorbed species in a full reaction.<sup>[38]</sup> Based on the linear energy relations, the search for new catalysts for ammonia synthesis can be facilitated by an initial screening without the need for performing full DFT calculations.<sup>[39]</sup> Since activation energies can be estimated from adsorption energies using linear relations, the scaling relations are often sufficient to be used as predictors of catalytic performance.

The adsorption energy can be given by DFT calculations with reasonable accuracy. The adsorption energy of hydrogen-containing species AH<sub>x</sub> (where A can be N, O, C, or S) is linearly correlated with the adsorption energy of atom A adsorbed onto metal surfaces<sup>[38]</sup>

$$\Delta E_{AH_x} = \alpha(x)\Delta E_A + \beta \quad (E1)$$

$$\alpha(x) = (x_{\max} - x)/x_{\max} \quad (E2)$$

where  $\alpha(x)$  is the slope of the scaling relation that closes to a constant for different surface types,  $\beta$  is a constant influenced by the geometric structure such as a close-packed surface or a stepped surface. The slope is given to a good approximation by the number of H atoms in AH<sub>x</sub>. The  $x_{\max}$  is the maximum number of H atoms that can bond to the central atom A ( $x_{\max} = 3$  for A = N,  $x = 0, 1$ , and 2 for N), and  $x$  is the actual number of H atoms that bond to A.

Such scaling relations have been used to generate free energy diagrams and volcano plots for electrochemical ammonia synthesis from N<sub>2</sub> reduction as a function of the N adsorption energy, and to predict the qualitative trends in catalytic activity of metal surfaces and other extended surfaces.<sup>[40–42]</sup> For multiple proton–electron transfer reactions, two (or more) intermediates

involved in the mechanism may bind to a catalyst in a similar manner so that there is very little room to adjust the energy differences between them, leading to a fundamental overpotential of the catalytic reaction in question. To reduce such a fundamental overpotential requested for NRR, emerging strategies are needed to overcome the scaling relations between key intermediates.<sup>[43]</sup>

### 3.2. NRR on Metal Surface

A pure metal surface is the simplest model to be analyzed for electrochemical ammonia formation. In a landmark work in 2012, Skúlason et al. evaluated the catalytic activity toward NRR on a range of flat and stepped transition metal surfaces by assuming that the activation energy scales with the free energy difference in each elementary step of NRR.<sup>[40]</sup> A volcano plot relating the theoretical limiting potential to the adsorption energies of nitrogen species on different metal surfaces is illustrated in **Figure 3a**, with Fe and Mo to be the most active surfaces for ammonia formation. However, these surfaces were predicted to be more active at promoting HER rather than NRR. Most of the metals investigated in this study, in particular, metals on the right legs of the volcano plot including Rh, Ru, Ir, Co, Ni, and Pt, are prone to be covered with H-adatoms instead of N-adatoms. As a result, there is a lack of available sites for N<sub>2</sub> adsorption and large overpotentials are requested to activate N<sub>2</sub>, which mainly leads to HER instead of NRR on most surfaces. Gratifyingly, the flat metal surfaces of some early transition metals such as Sc, Y, Ti, and Zr are expected to bind N-adatoms more strongly than H-adatoms, allowing for the reduction of N<sub>2</sub> to NH<sub>3</sub> at a theoretical applied bias of  $\sim$ 1.0 to  $-$ 1.5 V vs NHE. However, these early transition metal surfaces are also known to easily form oxides so that the question remains whether they can be effective NRR catalysts or not.

Transition metal nanoclusters with highly under-coordinated sites were found capable of enhancing the catalytic activity toward NRR. However, the competing HER still has a lower onset potential than NRR, suggesting that hydrogen evolution is the major challenge even for the very under-coordinated nanoclusters.<sup>[41]</sup> Mo and Fe are expected to be the most promising candidates for electrochemical NH<sub>3</sub> formation via the associative mechanism (Figure 3b). However, the active sites on catalyst surfaces can be blocked due to preferential adsorption of oxygen rather than nitrogen at the presence of water, thereby reducing the efficiency of these catalysts. A recent computational study showed that the Mo nanoclusters will preferentially bind oxygen over nitrogen and hydrogen at neutral bias.<sup>[44]</sup> Therefore, a negative potential ( $-$ 0.72 V or lower) is required to reduce oxygen off the surface and thereby to allow nitrogen molecules to be adsorbed to the surface.

The NRR mechanisms have been theoretically explored for nanoparticles that possess a variety of active sites as the catalyst. The NH<sub>3</sub> synthesis reaction via the Haber–Bosch process on the surface of Ru is generally believed to follow a dissociative pathway.<sup>[16]</sup> Notably, recent computational studies on stepped Ru surfaces have revealed a low activation barrier in the rate-determining step of the associative mechanism for stepped Ru surfaces,<sup>[45]</sup> and that the thermodynamic limiting potential of the associative pathways was similar to that of the dissociative

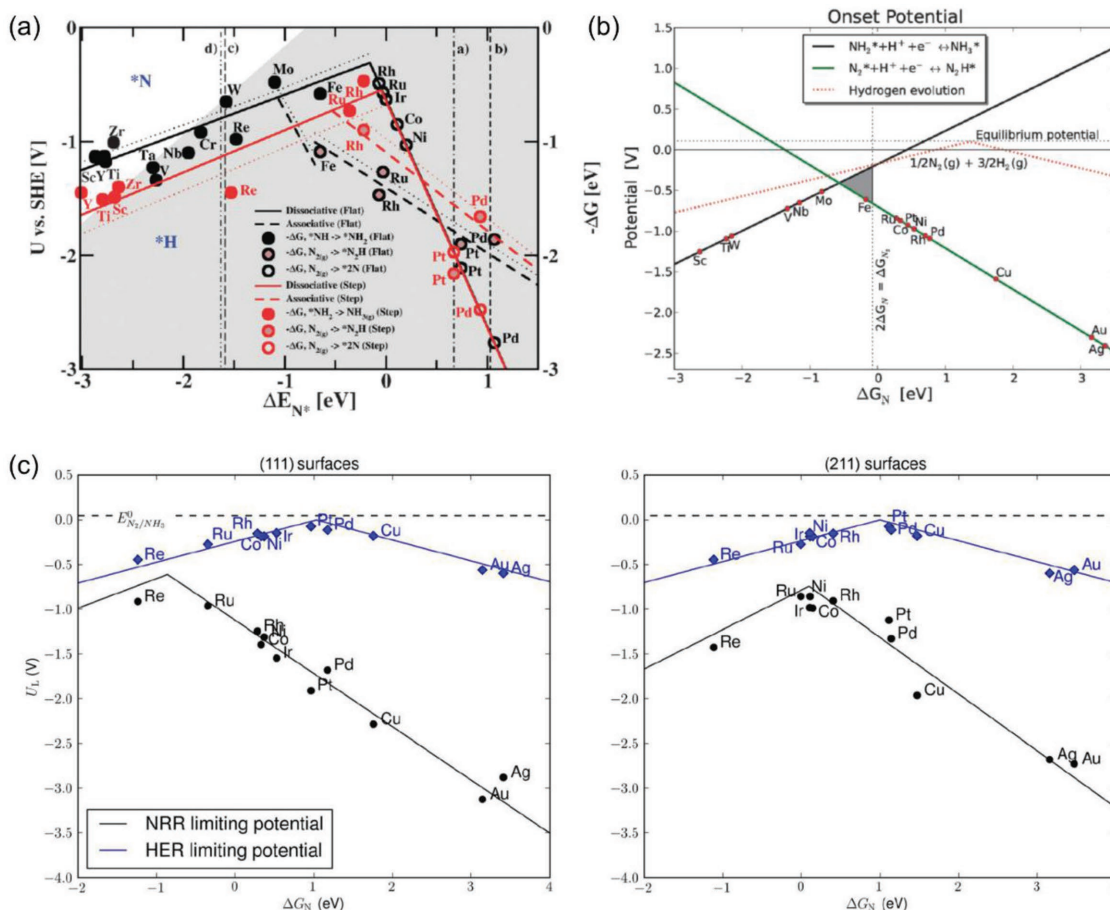


**Figure 3.** a) The dissociative (solid lines) and associative (dashed lines) mechanisms on both flat (black) and stepped (red) metal surfaces. Reproduced with permission.<sup>[40]</sup> Copyright 2012, The Royal Society of Chemistry. b) Volcano plot for the associative and dissociative mechanisms on metal nanocluster surfaces. Reproduced with permission.<sup>[41]</sup> Copyright 2013, The Royal Society of Chemistry. c) Comparison of limiting-potential volcanoes of HER (blue) and NRR (black) on different metal (111) (left) and (211) (right) surfaces. Reproduced with permission.<sup>[51]</sup> Copyright 2015, Wiley-VCH.

pathway.<sup>[46]</sup> Consequently, all possible reaction pathways in addition to the conventional associative and dissociative mechanisms should be taken into account to effectively predict ideal candidates and correctly understand NRR mechanisms. In a recent study, the NRR reaction rates were found to decrease in the order: Ru > Os > Rh, where the dissociation of  $N_2$  was assumed to be the rate-determining step.<sup>[47]</sup> Ru exhibited high activity because it satisfied the key factors including the activation energy barrier, surface vacant sites, and the number of step sites. However, the energy barrier for the first protonation of  $N_2$  can be substantially influenced by the partial coverage of H atoms on the Ru surfaces, leading to a change of the potential determining step and thereby an increase in the overpotentials.<sup>[46]</sup> Recently, an alternating pathway was proposed for NRR on Au surfaces with {730} crystal facets.<sup>[48]</sup> However, there is a lack of theoretical calculations for other reactive surfaces of Au nanoparticles or Au nanoclusters/Au single atom on supports toward NRR, albeit some recent experimental studies have shown that Au can be a promising candidate for electrocatalytic NRR at ambient conditions.<sup>[49,50]</sup>

The electrochemical reduction of  $N_2$  to  $NH_3$  on transition metal surfaces is severely limited by the linear scaling between the energetics of two key intermediates,  $*N_2H$  and  $*NH_2$ .<sup>[51]</sup> The  $*N$  binding energy was chosen for both NRR and HER because

the N and H adsorption energy scales. The overpotentials for NRR are consistently larger than those for HER (Figure 3c), which explains the lack of experimental observations of NRR on transition metals. The authors pointed out the challenge to design a system that can selectively stabilize  $*N_2H$  or destabilize  $*NH_2$ . One promising approach to meet this challenge may be the use of metal alloys, which can either be multifunctional in their interactions with the absorbed intermediates<sup>[52]</sup> or facilitate active sites in a beneficial way.<sup>[53]</sup> However, it should be noted that alloying may not break the scaling for  $*N_2H$  and  $*NH_2$ , as both of them form a bond to the surface similarly through a single N atom. Therefore, the active sites must be designed to change the binding configurations of these intermediates. For example, designing 3D active sites that can (de)stabilize one intermediate without affecting the other may help to mitigate the scaling limitation. Recently, a surface single-cluster catalyst with singly dispersed bimetallic  $M_1A_n$  sites was proposed for thermal conversion of  $N_2$  to  $NH_3$ .<sup>[54]</sup> Based on ab initio molecular dynamics simulations and static DFT calculations, isolated  $Rh_3Co_3$  cluster on CoO (011) surface was found to follow the enzymatic associative mechanism in an alternating pathway, with  $H_2$  activation on both metal sites to deliver the active H species. The charge buffer capacity of the doped metal M with low chemical valence can be

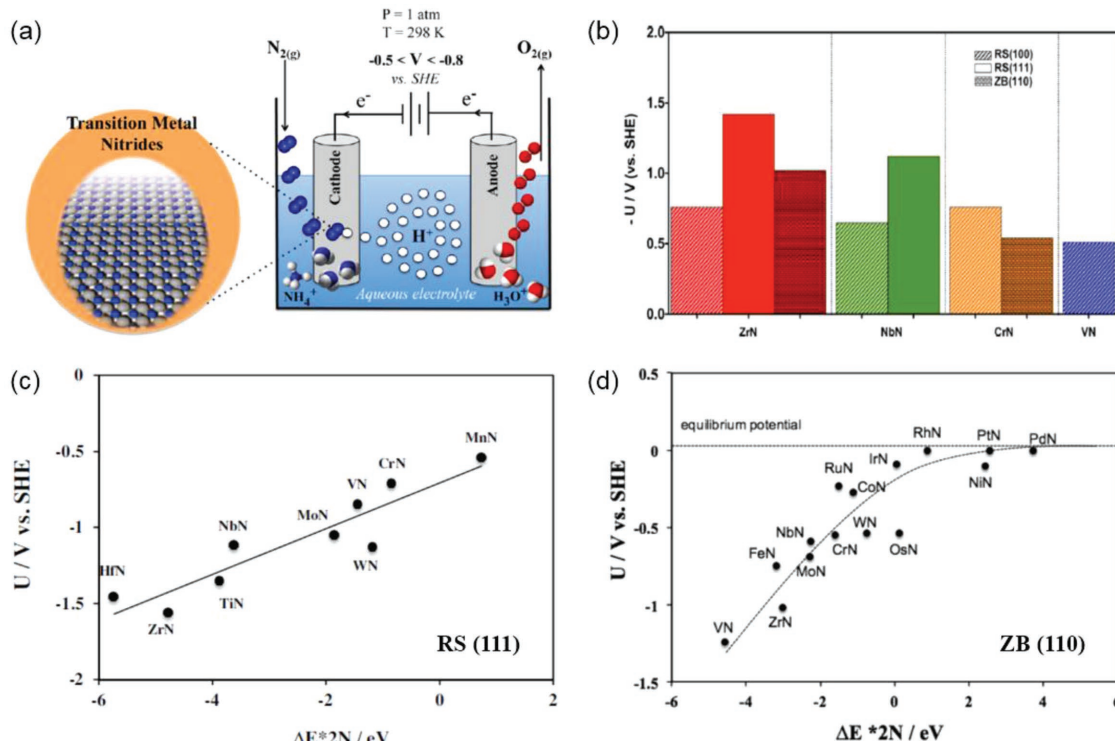


**Figure 4.** a) Schematic for electrochemical  $N_2$  reduction to  $NH_3$  on transitional metal nitrides (TMNs) at ambient conditions. b) Comparison of the proposed applied bias ( $U$ ) for electroreduction of  $N_2$  to  $NH_3$  via a MvK mechanism on stable facets of promising nitrides. Reproduced with permission.<sup>[60]</sup> Copyright 2015, American Chemical Society. c,d) Onset potential of ammonia formation as a function of the chemisorption energy of two N-adatoms in the N-vacancy on the RS (111) and ZB (110) facets of TMNs, respectively. Reproduced with permission.<sup>[61]</sup> Copyright 2016, Elsevier B.V. Reproduced with permission.<sup>[62]</sup> Copyright 2017, American Chemical Society.

used to tune the barriers in the alternating mechanism and to optimize the catalytic activity for  $NH_3$  formation. The idea proposed in this study can be well extended to guide catalyst design for electrochemical reduction of  $N_2$  to  $NH_3$ .

### 3.3. NRR on Metal Oxide/Nitride/Carbide Surface

On the background of electrochemical  $NH_3$  synthesis from  $N_2$  and steam electrolysis in molten hydroxide suspensions of nano- $Fe_2O_3$  reported by Licht et al.,<sup>[55]</sup> iron oxide has drawn strong attention as potential electrocatalyst toward NRR under more benign conditions. Given that hematite ( $\alpha$ - $Fe_2O_3$ ) is the most thermodynamically stable form of various iron oxides, DFT study was carried out on the electrochemical reactivity of hematite (0001) surfaces with either  $Fe-O_3-Fe$ - or  $Fe-Fe-O_3-$  termination.<sup>[56]</sup> The NRR mechanism was identified to follow the associative pathway, and the most demanding step is the addition of the first proton to the adsorbed molecular nitrogen, which requires an applied bias of  $-1.14\text{ V}$  ( $-1.84\text{ V}$  vs NHE) for the  $Fe-Fe-O_3-(Fe-O_3-Fe-)$  surface. This sheds a fresh light on the reactivity of Fe sites, and the predicted potential bias coincided with the experimental electrolysis potentials in Licht et al.'s work of electrochemical ammonia synthesis using  $Fe_2O_3$  nanoparticles in molten salt electrolytes at  $200\text{ }^\circ C$ .<sup>[55]</sup>

Very recently, the possibility of nitrogen activation for electrochemical  $NH_3$  synthesis under ambient conditions on the (110)

facet of several metal oxides in the rutile structure was investigated.<sup>[57]</sup> The most promising candidates turned out to be the (110) facets of  $NbO_2$ ,  $ReO_2$ , and  $TaO_2$  with low onset potentials of  $-0.57$ ,  $-1.07$ , and  $-1.21\text{ V}$  vs SHE, respectively. Though rutile  $IrO_2$  was found to have the highest reactivity toward NRR with an onset potential of  $-0.36\text{ V}$ , its surface was susceptible to be poisoned by adsorbed hydrogen atoms.

Metal nitrides can be more active than pure metal catalysts toward NRR than toward the competing HER. Abghouei et al. carried out a series of DFT-based analyses on a range of transition metal nitride surfaces toward NRR at ambient conditions in electrochemical media (Figure 4a).<sup>[58-62]</sup> The required onset potential was predicted via the MvK mechanism. The possibility of surface vacancy poisoning and the likelihood of catalyst decomposition and active sites regeneration under operating conditions were also scrutinized. The best material should have both high reactivity and good stability toward NRR. Mononitrides in both rocksalt (RS) and zincblende (ZB) structures were investigated. The most promising candidates turned out to be VN, CrN, NbN, and ZrN of the RS (100) structure with a low onset potential (Figure 4b). Among them, polycrystalline surfaces of VN exhibited a  $-0.5\text{ V}$  overpotential, which is possible to avoid both HER and catalyst decomposition.<sup>[60]</sup> Later, the same group used DFT calculations to screen a stable and active candidate toward NRR among a range of TMNs with either RS (111) facets or ZB (110) facets. In terms of the RS (111) facets, CrN, VN, MoN, WN, and NbN were predicted to have low onset potentials (Figure 4c).<sup>[61]</sup>

However, only NbN can regenerate itself and endure the catalytic cycle of nitrogen activation and NH<sub>3</sub> formation under operating conditions, and the others should decompose to the parental metals. In terms of the ZB (110) facets, RuN, CrN, and WN were predicted to be active at very low onset potentials (from -0.23 to -0.55 V vs RHE, Figure 4d).<sup>[62]</sup> They can be regenerated and sustain the catalytic cycle of electrochemical reduction of N<sub>2</sub> to NH<sub>3</sub> at ambient conditions. Such knowledge about the reactivity and stability of various mononitrides with different crystal structures and crystal facets is helpful to obtain polycrystalline materials with excellent NRR performance.

2D materials have been strongly considered in electrocatalysis applications. However, the possibility of 2D transition metal oxide/nitride/carbide as potential electrocatalysts toward NRR has rarely been analyzed from a theoretical perspective. Recently, Zhang and co-workers reported that pure MoN<sub>2</sub> nanosheets demonstrated excellent performance for N<sub>2</sub> adsorption and activation at room temperature, but required large energy input for surface refreshment.<sup>[63]</sup> Iron doping can improve the surface reactivity toward NRR with a calculated overpotential of 0.47 V.

Another computational study conducted by Azofra et al. suggests that 2D transition metal carbides (MXenes of the d<sup>2</sup>, d<sup>3</sup>, and d<sup>4</sup> series with the general formula M<sub>3</sub>C<sub>2</sub>) are promising for N<sub>2</sub> capture and reduction based on DFT investigations.<sup>[64]</sup> Chemisorbed N<sub>2</sub> on MXene nanosheets can elongate/weaken the N≡N triple bond, thus promoting its catalytic conversion into NH<sub>3</sub>. The overpotential can be as low as 0.64 V vs SHE in the case of V<sub>3</sub>C<sub>2</sub>.

### 3.4. NRR on Single-Atom-Based Surface

Single-atom catalysts (SACs) composed of isolated metal atoms anchored to support have emerged as promising candidates for heterogeneous catalysis. Distinguishing performances have been achieved for various electrocatalytic reactions.<sup>[65,66]</sup> However, the investigation on the reactivity of SACs for electrocatalytic N<sub>2</sub> reduction and NH<sub>3</sub> formation is very limited up to now.

In 2014, Tian and co-workers evaluated the catalytic profile of a molybdenum-graphene-based catalyst (Mo/N-doped graphene with a C<sub>33</sub>H<sub>15</sub>MoN<sub>3</sub> model, as shown in Figure 5a) for

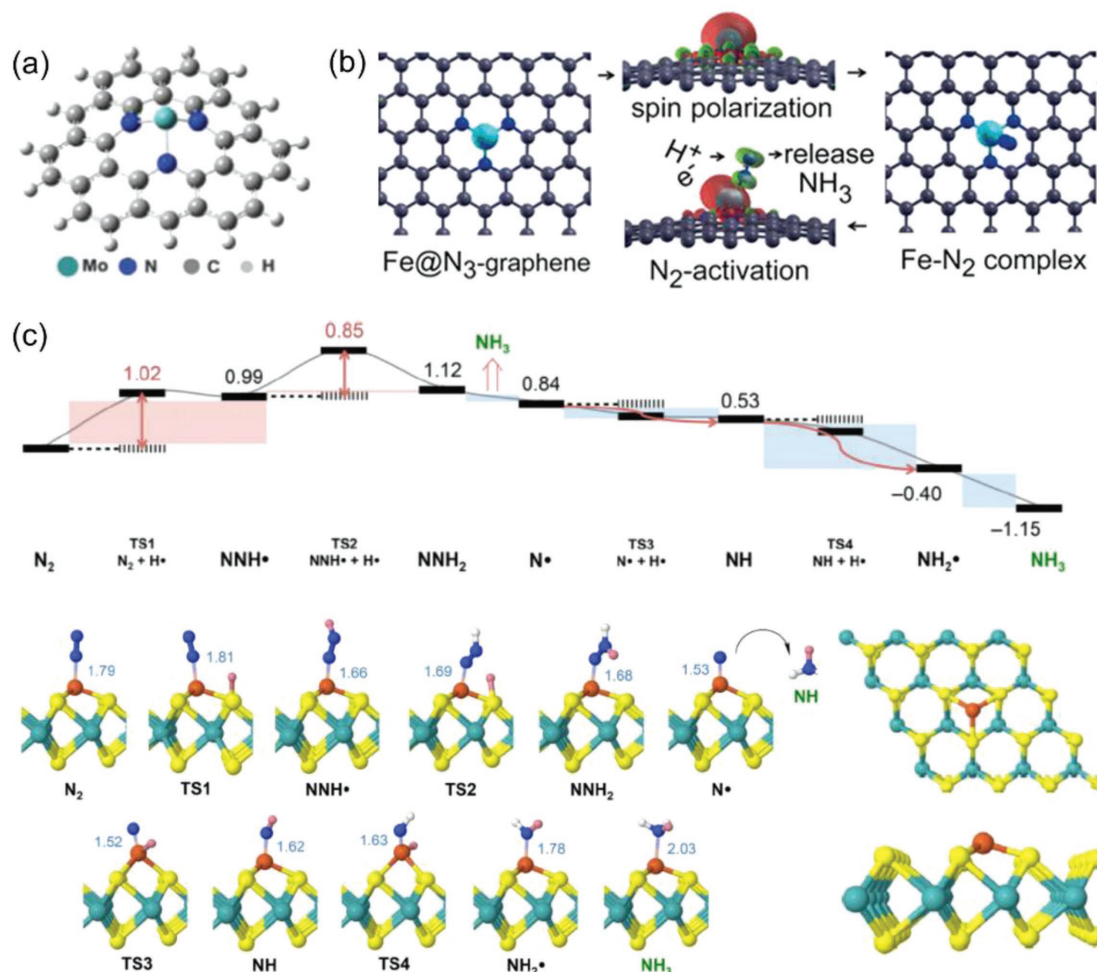


**Figure 5.** a) Model for the proposed Mo/N-doped graphene catalyst. Reproduced with permission.<sup>[67]</sup> Copyright 2014, The Royal Society of Chemistry. b) Schematic illustration of the FeN<sub>3</sub>-embedded graphene catalyst for NRR. Reproduced with permission.<sup>[68]</sup> Copyright 2016, American Chemical Society. c) Minimum Gibbs free energy path and structures of minima and transition states (TS) for NRR catalyzed by Fe deposited on MoS<sub>2</sub> 2D sheets. Reproduced with permission.<sup>[70]</sup> Copyright 2017, Wiley-VCH.

nitrogen fixation.<sup>[67]</sup> The system was designed in the hope that the merits of the following three parts could be combined: the Mo/N that acts as active centers, the graphene periphery region that acts as an electron donor or acceptor (i.e., an electron reservoir) and provides electrons for protonation and reduction, and the graphene body that acts as electron bridge for electron transportation. Later, FeN<sub>3</sub>-embedded graphene formed by embedding single Fe atom in the single vacancy formed in graphene by nitrogen doping was proposed for promoting N<sub>2</sub> adsorption and activation owing to the highly spin-polarized FeN<sub>3</sub> center (Figure 5b).<sup>[68]</sup> The synergistic effect between FeN<sub>3</sub> and graphene enabled the conversion of N<sub>2</sub> into NH<sub>3</sub> at room temperature, where the graphene acts as electron reservoir and the FeN<sub>3</sub> acts as N<sub>2</sub>-fixation sites and electron transmitters. Recently, Zhao and Chen investigated the potential of single transition metal atoms supported on defective boron nitride (TM-BN) monolayer with a boron monovacancy as electrocatalysts toward NRR.<sup>[69]</sup> The most active one is the single Mo atom supported by a defective BN nanosheet with a very low overpotential of 0.19 V for NRR at room temperature via an enzymatic mechanism. This superior catalytic performance can be ascribed to the synergistic role of the BN monolayer that acts as an electron reservoir and the MoN<sub>3</sub> moiety (i.e., Mo and its surrounding three N atoms) that serves as a transmitter to charge transfer between the adsorbed N<sub>x</sub>H<sub>y</sub> species and BN monolayer. Very recently, Azofra et al. investigated the feasibility of electrocatalytic reduction of N<sub>2</sub> to NH<sub>3</sub> on Fe-deposited 2D MoS<sub>2</sub> sheets in an aqueous media under mild conditions.<sup>[70]</sup> The material is calculated to spontaneously and selectively capture N<sub>2</sub>, relative to chemisorption of CO<sub>2</sub> and H<sub>2</sub>O. The limiting step is proposed to be the first proton–electron pair transfer for chemisorbed NNH\* radical, requiring an activation barrier of 1.02 eV (Figure 5c). Moreover, the lower binding energy between NH<sub>3</sub> and the material compared with that for N<sub>2</sub> capture indicates that the material can auto-regenerate, and thus be used for successive NRR cycles.

To date, there are very limited theoretical studies to examine the possibility of metal-free catalysts for electrochemical reduction of N<sub>2</sub> to NH<sub>3</sub>. Recently, the nitrogen activation and reduction capability of boron nitride nanotubes (BNNTs) have been investigated using DFT-based calculations.<sup>[33]</sup> The catalytic activity toward NRR was associated with the boron antisite, and the reaction energetics indicated that the distal mechanism is more favorable than the alternative mechanism for BNNTs under ambient conditions.

#### 4. Recent Experimental Advances in NRR

The pioneering experimental work on electrochemical ammonia synthesis from N<sub>2</sub> can be dated back to the 1960s, using nichrome cathodes and aluminum anodes, with titanium tetrakisopropoxide and aluminum chloride in 1,2-dimethoxyethane as the electrolyte.<sup>[71,72]</sup> Since the aluminum anode was consumed by conversion to aluminum nitride and then hydrolyzed, the process is not suitable for long-time reaction and large-scale production. In 1983, Sclafani et al. have demonstrated the feasibility of the reduction of N<sub>2</sub> over iron cathode

under ambient conditions in 6.0 M KOH aqueous electrolyte.<sup>[73]</sup> It was found that the NH<sub>3</sub> production rate depended on the temperature and the applied cathodic potential. The NH<sub>3</sub> production rate reached a peak value of 0.5 μmol h<sup>-1</sup> at -1.07 V vs saturated calomel electrode (SCE) with a NH<sub>3</sub> Faradaic efficiency of around 1% at 45 °C and 1 atm. Later, Furuya and Yoshioka reported electrochemical reduction of N<sub>2</sub> to NH<sub>3</sub> using gas-diffusion electrodes modified by Fe-phthalocyanine in various aqueous electrolytes at 25 °C and 1 atm.<sup>[74]</sup> Both the NH<sub>3</sub> production rate and the current efficiency (CE) dropped quickly after 10 min of electroreduction. The best performance was obtained in KOH electrolyte, with a CE of 0.11% after 10 min under galvanostatic conditions at -47.8 mA cm<sup>-2</sup>. In 1990, the NRR current efficiencies for electrocatalytic NH<sub>3</sub> production over Fe fine powder, various metal oxides, and metal sulfides, ZnSe, TiB, and SiC were investigated.<sup>[75]</sup> The CE was found to rely on the metal and its oxidation state. The metal sulfide seemed to be better than the corresponding oxides. Notably, a high CE of ≈2.24% was found on the ZnSe catalyst after 10 min at -0.5 V vs RHE, yet the CE quickly dropped to ≈0.1% after 30 min. These early experimental studies have found very low selectivity and poor stability toward ammonia formation.

It was not until the advent of the 21st century that electrochemical ammonia synthesis over heterogeneous catalysts under ambient conditions has aroused much more interest in the field. Attempts have been made using noble metal (such as Ru, Rh, Pt, and Au), transition metal (such as Fe and Ni), metal oxide (such as Fe<sub>2</sub>O<sub>3</sub>), metal-free materials, and their hybrids as catalysts. Different kinds of electrochemical cell have been developed with the use of either liquid or solid electrolytes. The electrochemical reactors reported in recent experimental investigations can be divided into four categories based on the differences in the cell configuration, as illustrated in Figure 6. In the following part, we summarize recent experimental advances with an emphasis on rational design of the whole electrochemical system including electrode materials, electrolytes, and cell configurations.

##### 4.1. Back-to-Back Cell

The back-to-back cell illustrated in Figure 6a with solid-state electrolyte has been widely used for solid-state electrochemical synthesis of NH<sub>3</sub> over a wide temperature range (25–800 °C). Details have been reviewed by Amar et al.,<sup>[3]</sup> Giddey et al.,<sup>[4]</sup> Kyriakou et al.,<sup>[19]</sup> and Garagounis et al.<sup>[76]</sup> The key components are two porous electrodes (anode and cathode) separated by a dense membrane. Among the various types of polymer membranes that can be used as electrolyte at ambient conditions, perfluorosulfonic acid proton-conducting membranes such as Nafion membranes from Dupont are the most popular. The benefits of using Nafion membranes include the high proton conductivity at ambient temperature and a good knowledge of proton exchange membrane fuel cell technology. In 2009, Xu et al. reported the use of perovskite oxide SmFe<sub>0.7</sub>Cu<sub>0.1</sub>Ni<sub>0.2</sub>O<sub>3</sub> cathode with Nafion membrane electrolyte and Ni–Ce<sub>0.8</sub>Sm<sub>0.2</sub>O<sub>2-δ</sub> anode for NH<sub>3</sub> synthesis from wet hydrogen and dry nitrogen at temperatures ranging from 25 to 100 °C.<sup>[77]</sup> The maximum NH<sub>3</sub> production rate of

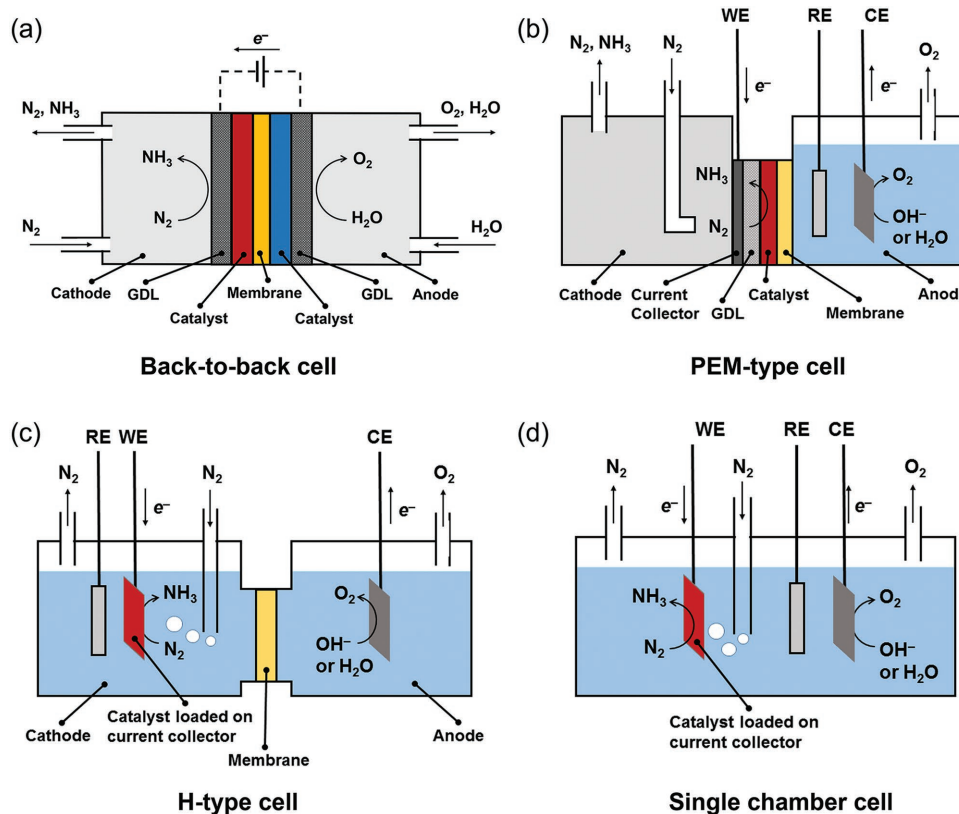


**Figure 6.** a-d) Schematics of different cell configurations for electrocatalytic NRR at ambient conditions. Note that the hydrogen evolution reaction is not shown here.

$1.13 \times 10^{-8} \text{ mol s}^{-1} \text{ cm}^{-2}$  (current density:  $3.5 \text{ mA cm}^{-2}$ ) was achieved at  $80^\circ\text{C}$ , with a FE of 90.4% at 2 V cell voltage. Later in 2010, using the same reactor configuration, a peak reaction rate of  $1.05 \times 10^{-8} \text{ mol s}^{-1} \text{ cm}^{-2}$  was observed on  $\text{Sm}_{1.5}\text{Sr}_{0.5}\text{NiO}_4$  cathode at  $80^\circ\text{C}$ .<sup>[78]</sup> The decrease of the  $\text{NH}_3$  production rate at temperatures higher than  $80^\circ\text{C}$  was ascribed to the decrease of water content. The lack of water reduces the proton conductivity of the Nafion membrane and hence reduces the ammonia production rate.

A significant contribution to the promotion of electrochemical ammonia synthesis directly from air and water was done by Tao and co-workers. They have demonstrated the use of platinum supported on carbon black ( $\text{Pt/C}$ ) catalyst as both the cathode and the anode electrode for  $\text{NH}_3$  production.<sup>[79]</sup> When water was used as the proton source, a maximum  $\text{NH}_3$  production rate of  $1.14 \times 10^{-9} \text{ mol s}^{-1} \text{ cm}^{-2}$  was obtained at a cell voltage of 1.6 V. The FE in both cases was smaller than 1.0% due to the competing hydrogen evolution. Later, Tao and co-workers investigated the ammonia formation rate using a  $\text{H}^+/\text{Li}^+/\text{NH}_4^+$  mixed conducting Nafion membrane and  $\text{Pt/C}$  electrodes.<sup>[80]</sup> The presence of  $\text{Li}^+$  ions hinders proton transfer and renders lower current at higher applied voltage. Increasing the reaction temperature leads to a higher ammonia formation rate, with the highest rate ( $9.37 \times 10^{-10} \text{ mol s}^{-1} \text{ cm}^{-2}$ ) and FE (0.83%) achieved at 1.2 V and  $80^\circ\text{C}$ . For these two studies, it has to be pointed out that the authors used a mixed  $\text{NH}_4^+/\text{H}^+$  conducting Nafion membrane to increase the chemical compatibility of the acidic Nafion membrane with  $\text{NH}_3$ . However, it is difficult to

completely rule out the contribution of  $\text{NH}_4^+$  ions dissolved from the treated Nafion membrane from the apparent  $\text{NH}_3$  production rates.

In contrast to proton exchange membrane such as Nafion, anion exchange membrane (AEM) selectively conducts hydroxide anion to the anode and enables a more advantageous basic cell environment. Recently, a team of researchers has proven the feasibility of AEM as electrolyte for  $\text{NH}_3$  generation.<sup>[81]</sup> Fe, FeNi, and Ni nanoparticles were applied as cathode catalysts, and their efficiency was tested for comparison. The initial efficiency of the Fe-only materials was as high as 41%, but quickly dropped to 1.6% in a matter of hours. In contrast, the Ni-only materials exhibited single-digit efficiencies (around 3%) initially, and the efficiency slowly increased with reaction duration. The estimated  $\text{NH}_3$  production rate of the Fe, FeNi, and Ni catalysts was in the range of  $(1.33\text{--}3.80) \times 10^{-12} \text{ mol s}^{-1} \text{ cm}^{-2}$  at 1.2 V and  $50^\circ\text{C}$ , which was lower than that of the  $\text{Pt/C}$  catalyst using PEM.

Apart from the use of solid-state electrolyte, the back-to-back type cell can also enable the use of liquid electrolyte, which extend the selection of catalysts and electrolytes. Very recently, electrochemical  $\text{NH}_3$  synthesis at low temperature ( $<65^\circ\text{C}$ ) and atmospheric pressure using nanosized  $\gamma\text{-Fe}_2\text{O}_3$  electrocatalysts incorporated into an AEM electrode has been reported (Figure 7).<sup>[82]</sup> In a half-reaction experiment conducted in a KOH electrolyte, the  $\gamma\text{-Fe}_2\text{O}_3$  electrode presented an FE of 1.9% and a weight-normalized activity of  $12.5 \text{ nmol h}^{-1} \text{ mg}^{-1}$  at 0.0 V vs RHE. In contrast, when the  $\gamma\text{-Fe}_2\text{O}_3$  nanoparticles were coated onto porous carbon

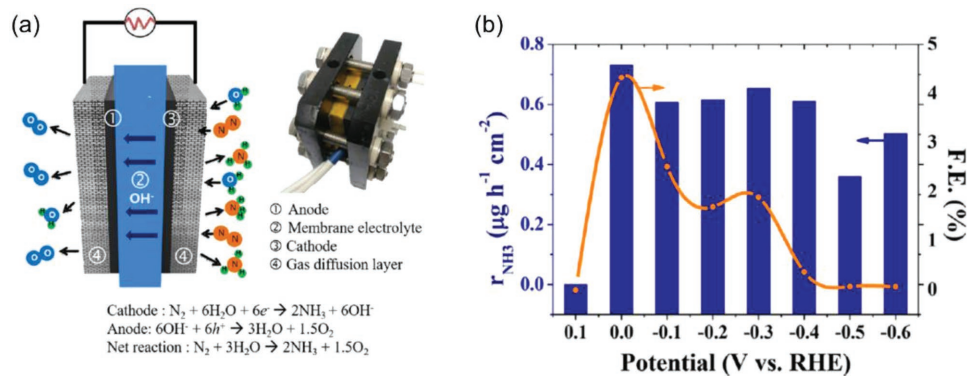


**Figure 7.** a) Electrochemical cell using an anion exchange membrane. b) Ammonia production rates and Faradaic efficiencies of a  $\gamma\text{-Fe}_2\text{O}_3$  catalyst in dependent with the applied potential. Reproduced with permission.<sup>[82]</sup> Copyright 2017, American Chemical Society.

paper to form an electrode, the weight-normalized activity for NRR was found to increase dramatically to  $55.9 \text{ nmol h}^{-1} \text{ mg}^{-1}$ .

#### 4.2. Polymer Electrolyte Membrane (PEM)-Type Cell

In 2000, Kordali et al. described electrochemical synthesis of  $\text{NH}_3$  from  $\text{N}_2$  gas and water using Ru catalyst deposited on carbon felt (Ru/C) in a polymer electrolyte membrane (PEM)-type cell (Figure 6b).<sup>[83]</sup> A 2.0 M KOH aqueous electrolyte was placed in the anode chamber and a Nafion membrane was employed to separate the cathode and anode chambers.  $\text{N}_2$  was supplied to the cathodic chamber and the  $\text{NH}_3$  produced was absorbed by a weak acid solution. Compared to the routine solid-state polymer membrane cell, the use of liquid electrolyte in the anode chamber has two advantages: 1) the convenience of adding a reference electrode that enables the measurement of the potential of the working electrode; and 2) the adequate wetting of the membrane that reduces the conductivity loss of the membrane. The  $\text{NH}_3$  formation rate is largely depended on the applied potential and the temperature. The  $\text{NH}_3$  production rate reached a peak value of  $1.30 \mu\text{g h}^{-1} \text{ cm}^{-2}$  at  $-1.02 \text{ V}$  vs Ag/AgCl at  $90^\circ\text{C}$  with a CE of 0.24%. In contrast, a much lower rate of  $0.21 \mu\text{g h}^{-1} \text{ cm}^{-2}$  and a CE of 0.28% were obtained at  $-1.10 \text{ V}$  at  $20^\circ\text{C}$ . It is worth noting that hydrazine was not detected in their experiments, indicating that  $\text{NH}_3$  was produced via a dissociative mechanism.

Very recently, Chen et al. demonstrated direct synthesis of  $\text{NH}_3$  from  $\text{N}_2$  and  $\text{H}_2\text{O}$  under room temperature and atmospheric pressure over iron oxide supported on carbon nanotubes ( $\text{Fe}_2\text{O}_3\text{-CNT}$ ) as cathode catalyst in an electrochemical cell similar to that shown in Figure 6b.<sup>[84]</sup>  $\text{NaHCO}_3$  aqueous electrolyte was placed in the anode compartment to generate the protons and electrons used on the cathode. A maximum ammonia yield of  $0.22 \mu\text{g h}^{-1} \text{ cm}^{-2}$  was obtained at  $-2.0 \text{ V}$  vs Ag/AgCl, whereas a maximum FE of 0.15% was obtained at  $-1.0 \text{ V}$  vs Ag/AgCl. The  $\text{Fe}_2\text{O}_3\text{-CNT}$  catalyst was fabricated by wet impregnation of o-CNTs with  $\text{Fe}(\text{NO}_3)_3$  and calcination at  $350^\circ\text{C}$ . The use of nitrate during the synthetic process might affect the  $\text{NH}_3$  measurement. Moreover, the iron oxide would probably be reduced during the activation stage of the electrocatalytic tests at the negative potential of  $-2.0 \text{ V}$  vs Ag/AgCl. Nevertheless, the structure and surface chemical state of the reduced iron oxide were not mentioned. Later, the same researchers further investigated the effects of iron content, electrolyte (type, pH, and concentration), and the applied voltage.<sup>[85]</sup> An optimal performance toward NRR was obtained on a 30 wt%  $\text{Fe}_2\text{O}_3\text{-CNT}$  catalyst, with an  $\text{NH}_3$  formation rate of  $1.06 \times 10^{-11} \text{ mol cm}^{-2} \text{ s}^{-1}$  and an  $\text{NH}_3$  FE of 0.164%. The electrolyte (type, pH, and concentration) demonstrated a minor effect on the  $\text{NH}_3$  formation rate, but a significant influence on the selectivity of  $\text{NH}_3$  formation (Figure 8a). A good stability was observed when the cell is set at a voltage of  $-1.0 \text{ V}$  vs Ag/AgCl. Importantly,  $\text{NH}_3$  was detected in both the cathode and the anode chambers, indicating the

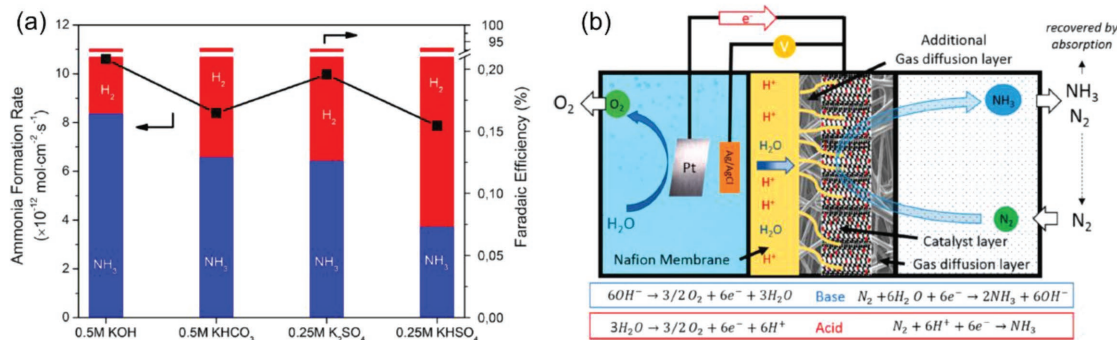


**Figure 8.** a) The average ammonia formation rate and Faradaic efficiency with different electrolyte. b) Schematic view of the improved design in the three-phase reactor for electrochemical ammonia synthesis. Reproduced with permission.<sup>[85]</sup> Copyright 2017, American Chemical Society.

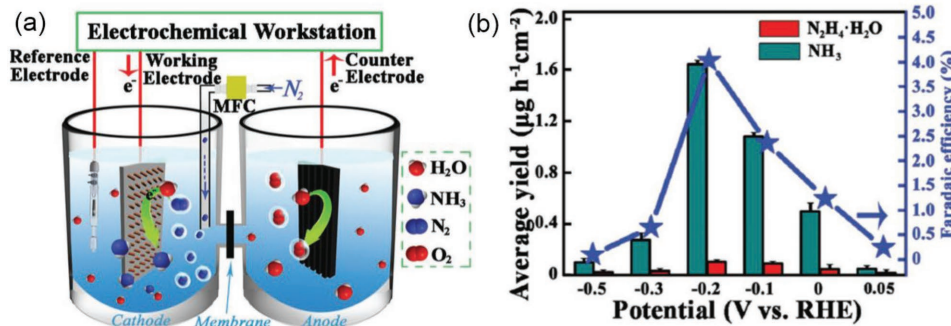


**Figure 9.** a) Schematic for electrocatalytic NRR (MFC is the mass flow controller, membrane is Nafion 211). b) Yield rate of ammonia (cyan), hydrazine hydrate (red) formation, and Faradic efficiency (blue) at each given potential. Reproduced with permission.<sup>[48]</sup> Copyright 2016, Wiley-VCH.

crossover of ammonia through the Nafion membrane. To mitigate the ammonia crossover effect, an additional gas diffusion layer was added between the electrocatalyst layer and the Nafion membrane (Figure 8b). Lately, our group has demonstrated that introducing more surface oxygen vacancies (OVs) to the commercial hematite ( $\alpha\text{-Fe}_2\text{O}_3$ ) nanoparticles can promote the electrocatalytic NRR at room temperature and atmospheric pressure. A PEM-type cell was employed with 0.10 M KOH as the electrolyte in the anode chamber. Considering the ammonia crossover effect, a maximum ammonia production rate of  $0.46 \mu\text{g h}^{-1} \text{cm}^{-2}$  and a maximum FE of 6.0% were achieved for the OV-enriched  $\alpha\text{-Fe}_2\text{O}_3$ /CNT catalyst when a voltage of  $-0.9 \text{ V}$  vs Ag/AgCl was applied.

#### 4.3. H-Type Cell with Liquid Electrolyte

Recently, Bao et al. demonstrated electrochemical reduction of  $\text{N}_2$  to  $\text{NH}_3$  at ambient conditions over tetrahedra gold nanorods (THH Au NRs enclosed by stepped 730 facet) in a double-chamber H-type cell (Figure 9a).<sup>[48]</sup> The two chambers of the H-type cell were separated by a Nafion membrane, and both were filled with 0.10 M KOH aqueous solution. An  $\text{NH}_3$  yield of  $1.648 \mu\text{g h}^{-1} \text{cm}^{-2}$  and an FE of 4.0% at  $-0.2 \text{ V}$  vs RHE were achieved (Figure 9b). The THH Au catalyst was proposed to follow an associative alternating pathway; in that both  $\text{NH}_3$  and  $\text{N}_2\text{H}_4 \cdot \text{H}_2\text{O}$  were detected in their experiment. Later, efforts were made to further improve the  $\text{NH}_3$  FE as well as to reduce the Au loading.<sup>[49,50]</sup> Another example using the H-type cell was the construction of a  $\text{Li}^+$  incorporation system in 0.50 M  $\text{Li}_2\text{SO}_4$  electrolyte.<sup>[86]</sup> Amorphous poly(*N*-ethyl-benzene-1,2,4,5-tetracarboxylic diimide) (PEBCD) was used as the catalyst to associate  $\text{Li}^+$  with the imide  $\text{C=O}$  groups on the surface. Nonetheless, it is unclarified that whether the leaching of N from the PEBCD would contribute to the amount of ammonia detected or not. Very recently, ultrathin Rh nanosheet nanoassemblies (Rh NNs) were used as electrocatalyst for NRR in a H-type cell separated by a Nafion 211 membrane.<sup>[87]</sup> A high  $\text{NH}_3$  yield of  $23.88 \mu\text{g h}^{-1} \text{mg}_{\text{cat}}^{-1}$  was achieved with no  $\text{N}_2\text{H}_4$  detected at low potential ( $-0.2 \text{ V}$  vs RHE). However, the  $\text{NH}_3$  FE of Rh NNs was only 0.217% at  $-0.2 \text{ V}$  vs RHE, much lower than that of the previously reported THH Au catalyst due to the severe competing HER. Additionally, the amount of ammonia measured was from the cathodic chamber and the absorber, without

considering ammonia crossover to the anodic chamber. Nonetheless, since the catalyst was synthesized from an inorganic polymer  $\text{RhCl}_3\text{-K}_3\text{Co}(\text{CN})_6$  cyanogel, it remains unknown that whether the  $\text{CN}^-$  would lead to ammonia contamination during the electrocatalytic measurements.

In the H-type cell, both the working electrode and the reference electrode are located in the cathode chamber, making it more accurate to measure the applied potentials, exerted on the working electrode than using the PEM-type cell, in which the reference electrode has to be placed in the anode chamber filled with electrolyte. However, the H-type cell with Nafion membrane as the separator also exhibits similar ammonia/ammonium crossover effect as in the case of PEM-type cell. Therefore, it is recommended that both the cathode electrolyte and the anode electrolyte have to be taken to measure the total ammonia/ammonium production. Moreover, membranes that can largely prevent the ammonia/ammonium crossover effect or additional antidiiffusion layers should be used to avoid possible ammonia/ammonium oxidation at the anode.

#### 4.4. Single Chamber Cell with Liquid Electrolyte

In 2006, the Köleli and Röpke have investigated electrochemical  $\text{NH}_3$  production in aqueous systems on a polyaniline electrode using a single chamber cell which was able to operate under high pressure (Figure 10a).<sup>[88]</sup> This is the first report of electrocatalytic  $\text{NH}_3$  synthesis on a metal-free catalyst. The  $\text{NH}_3$  yield and CE depended on the applied pressure on the polyaniline film coated on a Pt plate in methanol/ $\text{LiClO}_4/\text{H}_2\text{SO}_4$  electrolyte at ambient temperature. The  $\text{NH}_3$  yield and the CE obtained at atmospheric pressure were much smaller than those obtained at high pressure (Figure 10b). The  $\text{NH}_3$  formation rate was  $2.25 \times 10^{-7} \text{ mol h}^{-1} \text{cm}^{-2}$  at a potential of  $-0.12 \text{ V}$  vs NHE at 1 bar and  $25^\circ\text{C}$ . In 2010, Köleli and Kayan tested  $\text{NH}_3$  formation on a polypyrrole electrode and reported a  $10 \mu\text{mol L}^{-1} \text{NH}_3$  concentration after 5 h electrolysis duration in aqueous 0.10 M  $\text{Li}_2\text{SO}_4/0.03 \text{ M H}^+$  electrolyte at  $-0.165 \text{ V}$  vs NHE at atmospheric pressure and room temperature.<sup>[89]</sup> The first step of electrochemical  $\text{N}_2$  reduction on the polypyrrole electrode was proposed to be a Volmer reaction where  $\text{H}^+$  in the aqueous solution forms  $\text{H}_{\text{ad}}$ . Then  $\text{H}_{\text{ad}}$  is added on the  $\text{N}_2$  molecules adsorbed on the polymer via hydrogen bonds to generate  $\text{NH}_3$ . These two studies demonstrated the possibility

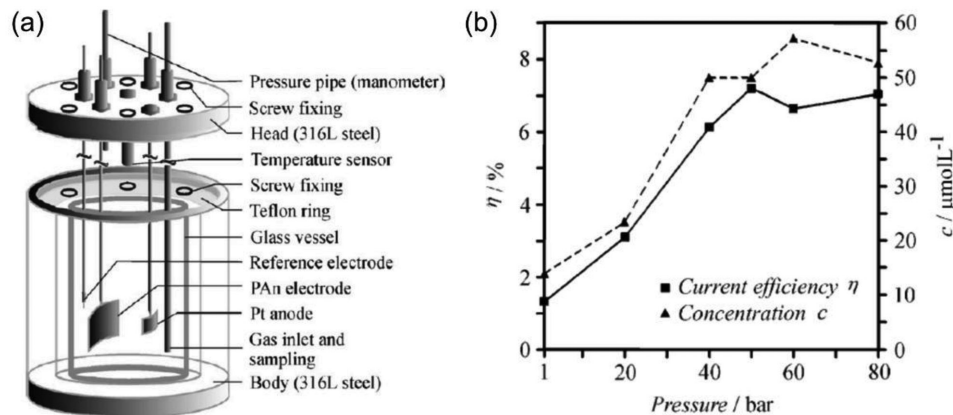


**Figure 10.** a) High-pressure single chamber cell used for electrocatalytic ammonia synthesis. b) Current efficiency versus pressure diagram of the  $\text{NH}_3$  formation on a polyaniline electrode (1.5 mm) after 5 h electrolysis time, at  $-0.12$  V vs NHE and  $25$   $^\circ\text{C}$ . Reproduced with permission.<sup>[88]</sup> Copyright 2005, Elsevier B.V.

of electrochemical reduction of dinitrogen on nonmetal materials. It has to be pointed out that both polyaniline and polypyrrole are amine-containing polymers, which bring forward the question that whether the nitrogen in the materials participates in the NRR process and contributes to the measured  $\text{NH}_3$  or not.

In 2015, Wessling and co-workers galvanically deposited Rh and Ru on randomly structured Ti felts as electrocatalyst for NRR.<sup>[90]</sup> The tests were conducted in a single chamber cell with  $0.50$  M  $\text{H}_2\text{SO}_4$  as an electrolyte at  $30$   $^\circ\text{C}$ . The  $\text{NH}_3$  production rate was found to be eight times higher for Ru ( $1.2 \times 10^{-10}$  mol  $\text{s}^{-1}$   $\text{cm}^{-2}$ ) than for Rh ( $1.5 \times 10^{-11}$  mol  $\text{s}^{-1}$   $\text{cm}^{-2}$ ). However, it has to be mentioned that a Ru complex containing  $\text{NH}_4^+$  was used for the galvanic deposition of Ru. Possible presence of the residual  $\text{NH}_4^+$  in the electrochemical system might affect the measurement of  $\text{NH}_3$  from  $\text{N}_2$  reduction.

The main problems for the aqueous electrolyte-based electrochemical cell for NRR are the dominant  $\text{H}_2$  evolution occurred at the same region of potential for NRR and the very limited  $\text{N}_2$  solubility in aqueous media. Attempts to suppress HER using a mixture of electrolytes and Ni catalysts have been made by

Kim et al.<sup>[91,92]</sup> In a single chamber cell system (Figure 11a), a mixture of 2-propanol/water (9:1, v/v) was used since the addition of 2-propanol can suppress HER.<sup>[91]</sup> The concentration of  $\text{H}_2\text{SO}_4$  and the applied current density were found to influence the  $\text{NH}_3$  yield and the  $\text{NH}_3$  FE. Optimized conditions led to an  $\text{NH}_3$  formation rate of  $1.54 \times 10^{-11}$  mol  $\text{s}^{-1}$   $\text{cm}^{-2}$  and an FE of  $\approx 0.9\%$ . However, the 2-propanol was found to be instable in a reducing environment and led to FE far from optimal (less than 1%). Comparatively, in a H-type cell system (Figure 11b), ethylenediamine (EDA) in  $0.10$  M LiCl was employed as the cathodic electrolyte and  $0.05$  M  $\text{H}_2\text{SO}_4$  as the anodic electrolyte.<sup>[92]</sup> A high  $\text{NH}_3$  FE of  $17.2\%$  was obtained, producing  $7.73 \times 10^{-7}$  mol  $\text{NH}_3$  for 1 h electrolysis at a cell voltage of  $1.8$  V. EDA was found to be a promising solvent for electrochemical  $\text{NH}_3$  synthesis under ambient conditions. However, optimizing of the reactor configuration is requested to suppress its crossover effect. Importantly, it is worth noting that EDA, with the formula  $\text{C}_2\text{H}_4(\text{NH}_2)_2$ , may as well lead to the formation of  $\text{NH}_3$ . When Ar was purged instead of  $\text{N}_2$ ,  $\text{NH}_3$  began to be detected from 40 min, which was a false-high  $\text{NH}_3$  resulted from EDA crossover and oxidation. Hence, the formation of  $\text{NH}_3$  with Ar was

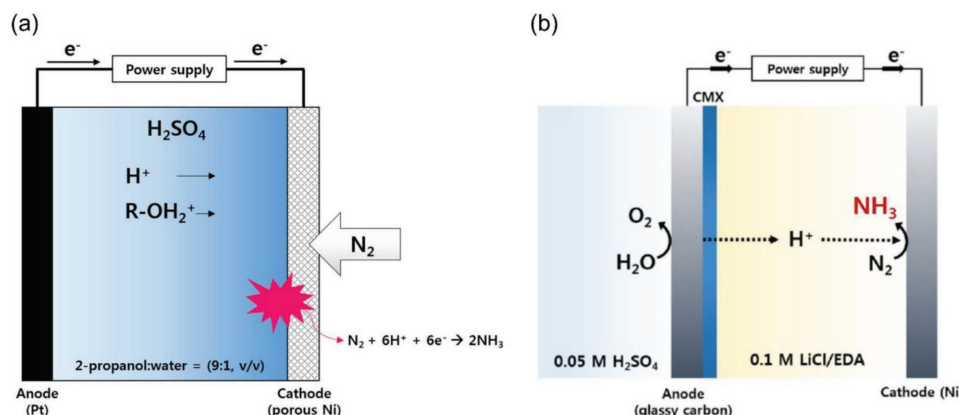


**Figure 11.** a) Schematic of NRR over porous Ni cathode in a single chamber cell with a mixture of 2-propanol/deionized water as the electrolyte medium. b) Schematic of NRR over Ni wire cathode in a double-chamber cell filled with different electrolytes. Reproduced with permission.<sup>[91,92]</sup> Copyright 2016, The Electrochemical Society.

used as a baseline to obtain meaningful values of NH<sub>3</sub> synthesized from N<sub>2</sub> reduction. To prove that the supplied N<sub>2</sub> did turn into NH<sub>3</sub>, electrocatalysis was carried out in the alternating presence of Ar and the isotope <sup>15</sup>N<sub>2</sub>.

A disadvantage of the single chamber cell is that gaseous products at the anode may be oxidized at the anode. In contrast, the double-chamber cell with an ion-exchange membrane as the separator makes it possible to prevent further oxidation of the gaseous products by only allowing the transfer of desired ions. Moreover, different electrolytes can be incorporated in the cathodic and anodic chambers of the H-type cell so that reactions on the cathode can be tuned independently with little influence to the anode.

## 5. Strategies for an Active, Selective, and Efficient Electrochemical System

The major problem of current NRR is associated with a lack of effective electrocatalysts for electrochemical N<sub>2</sub> reduction and NH<sub>3</sub> formation under ambient conditions. Large overpotentials for N<sub>2</sub> reduction and very low Faradaic efficiencies toward NH<sub>3</sub> formation are always detected. The thermodynamics of NRR suggest that the electrochemical reduction of N<sub>2</sub> should proceed at negative potentials that are dominated by the competing HER, leading to a tough selectivity issue. On the other hand, owing to the complicated electrochemical system, the key factors that affect the NH<sub>3</sub> formation rate are also quite complex, including the electrode materials (catalysts, additives, current collectors, etc.), the conductivity of the working electrode, the electrolyte, the reactor configuration, temperature, the applied potential/current, the N<sub>2</sub> partial pressure and the proton flux, etc. Hence, the experimentally measured NH<sub>3</sub> formation rates used to evaluate the NRR activity of the electrocatalysts actually reflect the properties of the whole electrochemical system. The NH<sub>3</sub> FE or CE which is employed to evaluate the NH<sub>3</sub> selectivity also strongly depends on the properties of the whole electrochemical system.

Up to now, various strategies to either suppress or circumvent HER have been proposed for electrochemical NH<sub>3</sub> synthesis aiming at boosting the activity and increasing the selectivity toward NRR. These strategies can be roughly generalized to follow three routes: 1) electrocatalyst design with altered intrinsic reactivity and selectivity toward NRR, 2) interface engineering with limited proton/electron transfer rate beneficial for NRR, and 3) decoupled N<sub>2</sub> fixation and NH<sub>3</sub> production to circumvent HER.

### 5.1. Boosting NRR by Rational Catalyst Design

Rational design of the electrocatalysts is requested to improve their intrinsic catalytic reactivity and selectivity toward NRR. Various strategies include crystal facets effect,<sup>[48,93]</sup> crystal size effect,<sup>[49]</sup> and amorphous phase effect<sup>[50]</sup> have been demonstrated on metal catalysts. For instance, on the aspect of the crystal facet effect, Yang et al. reported an improved catalytic activity toward NRR with the increase of (110) orientation value of Mo nanofilm.<sup>[93]</sup> A maximum NH<sub>3</sub> formation

rate of  $3.09 \times 10^{-11}$  mol s<sup>-1</sup> cm<sup>-2</sup> was achieved at -0.49 V vs RHE and a maximum FE of 0.72% was obtained at -0.29 V vs RHE in 0.010 M H<sub>2</sub>SO<sub>4</sub> electrolyte. To demonstrate the size effect of Au, Shi et al. compared the NRR performance of tannic acid (TA)-reduced ( $\approx$ 0.5 nm) Au/TiO<sub>2</sub>, NaBH<sub>4</sub>-reduced ( $\approx$ 4 nm) Au/TiO<sub>2</sub>, and photoreduced ( $\approx$ 37 nm) Au/TiO<sub>2</sub> and found that the TA-reduced Au/TiO<sub>2</sub> exhibited the highest NH<sub>3</sub> yield (21.4 µg h<sup>-1</sup> mg<sup>-1</sup><sub>cat</sub> at -0.2 V vs RHE) with a high FE of 8.11%.<sup>[49]</sup> Reducing the size of metal nanoparticles induces the creation of low-coordination sites apart from the original close-packed sites, thereby resulting in the decoupling of site preference of different adsorbates and thus facilitates NRR at a low overpotential. In terms of the amorphization strategy, defective sites can be induced to promote the catalytic activity. For instance, Li et al. synthesized amorphous Au/CeO<sub>x</sub>-reduced graphene oxide (RGO) hybrid catalysts with an Au loading of 1.31 wt%, achieving an FE of 10.10% at -0.2 V vs RHE.<sup>[85]</sup> The presence of CeO<sub>x</sub> was found to be necessary for the formation of amorphous Au, which possessed a higher concentration of unsaturated coordination sites toward NRR, thereby improving the Faradaic efficiency. In another case, an amorphous Bi<sub>4</sub>V<sub>2</sub>O<sub>11</sub>/CeO<sub>x</sub> was reported to show excellent NRR performance with a high NH<sub>3</sub> yield (23.21 µg h<sup>-1</sup> mg<sup>-1</sup><sub>cat</sub> at -0.2 V vs RHE) and a high FE (10.16%).<sup>[94]</sup> The amorphous Bi<sub>4</sub>V<sub>2</sub>O<sub>11</sub> with multiple defects served as the active ingredient, whereas the CeO<sub>x</sub> triggered the formation of the amorphous phase and participated in establishing band alignment for charge transfer. It is worth noting that NH<sub>4</sub>VO<sub>3</sub> and polyvinylpyrrolidone were used to synthesize the material, which causes ammonia contamination during the electrochemical measurements.

In terms of the defect engineering strategy, N-doped porous carbon (NPC) was reported recently as a cost-effective electrocatalyst toward NRR under ambient conditions.<sup>[95]</sup> Pyridinic nitrogen and pyrrolic nitrogen were proposed to be the active sites for ammonia synthesis. Additionally, the porous structure of NPC favored the trapping of N<sub>2</sub> and stabilizing of the intermediates. Again, once precursor containing CN<sup>-</sup> is applied, the accurate measurement of the generated NH<sub>3</sub> from N<sub>2</sub> is quite challenging. Moreover, it is unclear that whether the nitrogen atoms in the NPC participate in the NRR or not.

The effective tailoring of surface OVs on metal oxide catalysts can regulate the surface electronic structure, which is beneficial to improve the NRR catalytic activity.<sup>[56,96]</sup> The surface nitrogen vacancies of metal nitrides play a key role for electrochemical N<sub>2</sub> reduction. Theoretical calculation has demonstrated the importance of surface nitrogen vacancy regeneration to maintain the reactivity for N<sub>2</sub> reduction. Previous DFT calculations shed light on the effect of surface defects, crystal structure, and crystal facets on rational synthesis of metal oxide and metal nitride catalysts.<sup>[56,60,62,97]</sup>

In recent years, strain engineering for tuning the electronic structure of catalysts has become an effective strategy to enhance the electrocatalytic activity toward ORR/OER/HER,<sup>[98-100]</sup> and methanol oxidation reaction (MOR).<sup>[101]</sup> For instance, **strain-induced splitting of the e<sub>g</sub> orbitals can dramatically affect the catalytic activity of perovskite oxide LaNiO<sub>3</sub>**.<sup>[98]</sup> Another study demonstrated that the introduction of tensile strain into the surface of CoO can lead to the creation of a large quantity of oxygen vacancies that facilitate water dissociation.<sup>[99]</sup>

Recently, photoreduction of  $N_2$  to  $NH_3$  in water at 25 °C under visible-light irradiation has been achieved using **ultrathin layered double hydroxide (LDH) photocatalysts**.<sup>[102]</sup> The excellent photocatalytic activity of the LDH nanosheets toward NRR was ascribed to an abundance of OVs that enhanced the adsorption and activation of  $N_2$  and  $H_2O$ , as well as the severely distorted structure and compressive strain in the LDH nanosheets that enhanced  $N_2$  chemisorption and thereby promoted  $NH_3$  formation. Therefore, it is reasonable to believe that tuning the surface reactivity of transitional metal oxides by controlling the strain and surface defects might as well induce modulations in atomic and electronic structures to facilitate electrocatalytic NRR.

Recently, **anion regulation** has emerged as an effective way to improve the OER activity of transition metal compounds, owing to the composition–structure regulating effect.<sup>[103]</sup> For instance,  $O^{2-}$  or  $OH^-$  is capable of replacing the original anions of transition metal-based catalysts during the electrocatalytic process in alkaline electrolytes. Such a phenomenon indicated that most transition metal-based compounds (including chalcogenides, nitrides, and phosphides) are actually anion-regulated when catalyzing the reaction, and such anion regulation can be effective in enhancing the OER activity. A recent study on anion regulation of NiFe (oxy)sulfide catalysts showed that the material structure and electronic structure can be modulated via **changing the sulfide content of the NiFe (oxy)sulfide catalysts**, thereby significantly promoting their OER reactivity.<sup>[104]</sup> Strategies including crystal facet engineering,<sup>[105,106]</sup> defect engineering,<sup>[107–109]</sup> strain engineering,<sup>[110]</sup> and anion regulation for ORR/OER<sup>[111,112]</sup> are expected to inspire insights into rational design of effective NRR electrocatalysts.<sup>[113]</sup>

Metal–organic frameworks (MOFs) and covalent–organic frameworks (COFs) that represent a platform with ordered and metrically defined organic backbones allow for the integration of well-defined, highly selective molecular catalysts. These reticular materials are capable of being tailored in terms of pore structure and specific surface area, allowing for facile mass transport. The electron transport issue is solved by growing the MOF/COF films on conductive substrates. Hence, both the selectivity and the efficiency can be improved.<sup>[115]</sup> Moreover, the functional groups and the metal ion centers in MOFs/COFs can be directly designed as effective catalytic active sites. A recent study employing a series of MOFs (i.e., MOF(Fe), MOF(Co), and MOF(Cu)) as electrocatalysts toward NRR exhibited a high ammonia formation rate of  $2.12 \times 10^{-9} \text{ mol s}^{-1} \text{ cm}^{-2}$  and an FE of 1.43% at 1.2 V and 90 °C for the MOF(Fe) catalyst.<sup>[114]</sup> Moreover, it has been shown that COF catalysts can meet the criteria for high activity, high selectivity, and high efficiency.<sup>[115]</sup> COFs are unique primarily owing to their highly designable skeletons and pores using topology diagrams. COFs offer confined molecular spaces for mechanistic studies of correlated organic  $\pi$ -systems in which the confined space triggers interactions with electrons, holes, spins, ions, and molecules.<sup>[116]</sup> Hence, unique physical, chemical, and electrochemical properties can thus be tuned, thereby contributing to the design of active, selective, and efficient NRR catalysts. To improve the efficiency of the system, the interplay between the mass and electron transport should be regulated. The mass transport can be optimized by tuning the pore structure and film thickness of

the electrode based on porous materials, whereas electron transport to active sites can be optimized by enhancing the charge carrier mobility in the interconnected electron pathways.<sup>[115]</sup>

To achieve both high activity and selectivity for electrochemical reduction of  $N_2$  to  $NH_3$ , the electrocatalysts shall be deviated from the scaling relations shown for metals. Montoya et al. proposed strategies such as surface functionalization with co-adsorbates, utilization of promoters and electrolytes to tune the adsorption energies of the key adsorbates involved in NRR,<sup>[51]</sup> which will be discussed in Section 5.2. On the other hand, strategies to break the scaling relations to enhance  $CO_2$  electrochemical reduction reactions ( $CO_2$ ERR) are very helpful.<sup>[117]</sup> For instance, doping p-states' elements into the metal catalysts by modulating reaction energetics via p-block elements and enhancing catalytic activity well beyond modulations via d-block dopants are also proposed.<sup>[118]</sup>

## 5.2. Suppressing HER at the Catalyst/Electrolyte Interface

According to the analysis made by Nørskov and co-workers, limiting either proton or electron availability at the catalyst surface can be a promising way to retard HER and improve NRR selectivity.<sup>[117]</sup> Their qualitative model suggested that HER should always dominate at normal proton concentrations outside a metal surface. If there are very few protons or electrons provided, NRR preferentially occurs. This hypothesis is in agreement with recent experimental studies. For instance, a promising strategy to suppress HER via deliberate design of the catalyst/electrolyte surface in aqueous media has been demonstrated recently.<sup>[86]</sup> A  $Li^+$ -incorporation system was constructed by associating  $Li^+$  in the electrolyte with the imide  $C=O$  groups on the surface of PEBCD. Owing to the active  $O-Li^+$  sites in PEBCD, either the Tafel or the Heyrovsky reaction path for HER can be obstructed, resulting in a larger potential window to achieve a higher-selectivity NRR (Figure 12). The best  $NH_3$  formation rates and the corresponding  $NH_3$  FE are obtained as  $1.58 \mu\text{g h}^{-1} \text{ cm}^{-2}$  and 2.85%, respectively.

To limit the proton concentration available to the catalyst surface, a mixture of electrolyte was often used for aqueous systems.<sup>[92]</sup> Recently, a polymer-based gel electrolyte was employed for NRR at low temperature and pressure for the purpose of controlling the rate of HER by limiting the water transport.<sup>[119]</sup> Extremely, ionic liquid electrolyte with trace amounts of water can serve as an excellent electrolyte for HER suppression owing to limitation of the proton transfer rate. Very recently, Macfarlane and co-workers reported the use of  $[C_4mpyr][eFAP]$  and  $[P_{6,6,6,14}][eFAP]$  with trace amounts of water (as the proton source) and Fe-based catalysts deposited on fluorine-doped tin oxide glass (FTO), stainless steel (SS) mesh, and nickel foam (NF) for NRR at ambient conditions (Figure 13a,b).<sup>[120]</sup> The FE in  $[C_4mpyr][eFAP]$  is lower than that in  $[P_{6,6,6,14}][eFAP]$ , coinciding with the differences in  $N_2$  solubility, whereas the  $NH_3$  yield in  $[C_4mpyr][eFAP]$  is higher due to its lower viscosity (Figure 13c,d). The highest FE of 60% was obtained on FTO- $[P_{6,6,6,14}][eFAP]$  with a very low  $NH_3$  yield due to a very tiny catalyst loading, whereas the highest  $NH_3$  yield ( $14 \text{ mg h}^{-1} \text{ m}^{-2}$ ) was obtained on SS- $[C_4mpyr][eFAP]$  with a moderate FE of 30%. It is worth noting that the purity of the gas stream was analyzed,

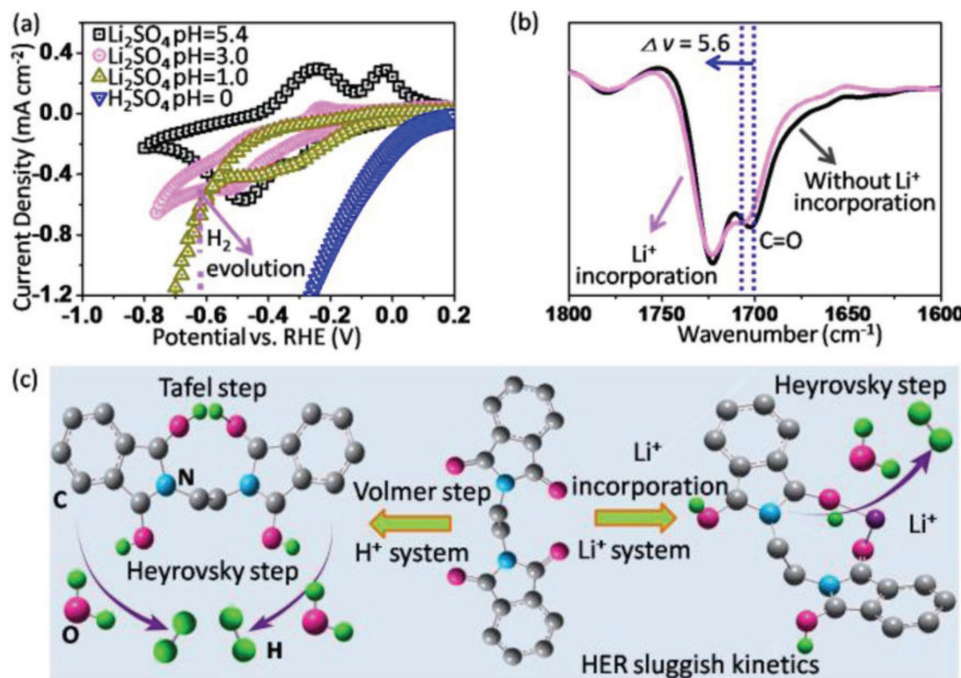


**Figure 12.** a) CV curves for the PEBCD/C electrode recorded in 0.50 M Li<sub>2</sub>SO<sub>4</sub> electrolytes with various pH values and the C cloth electrode in 0.50 M H<sub>2</sub>SO<sub>4</sub> electrolyte. b) FTIR spectra of PEBCD before and after Li<sup>+</sup> incorporation. c) Schematic illustration of Li<sup>+</sup> system to obstruct either the Tafel or the Heyrovsky reaction path for HER. Reproduced with permission.<sup>[86]</sup> Copyright 2017, American Chemical Society.

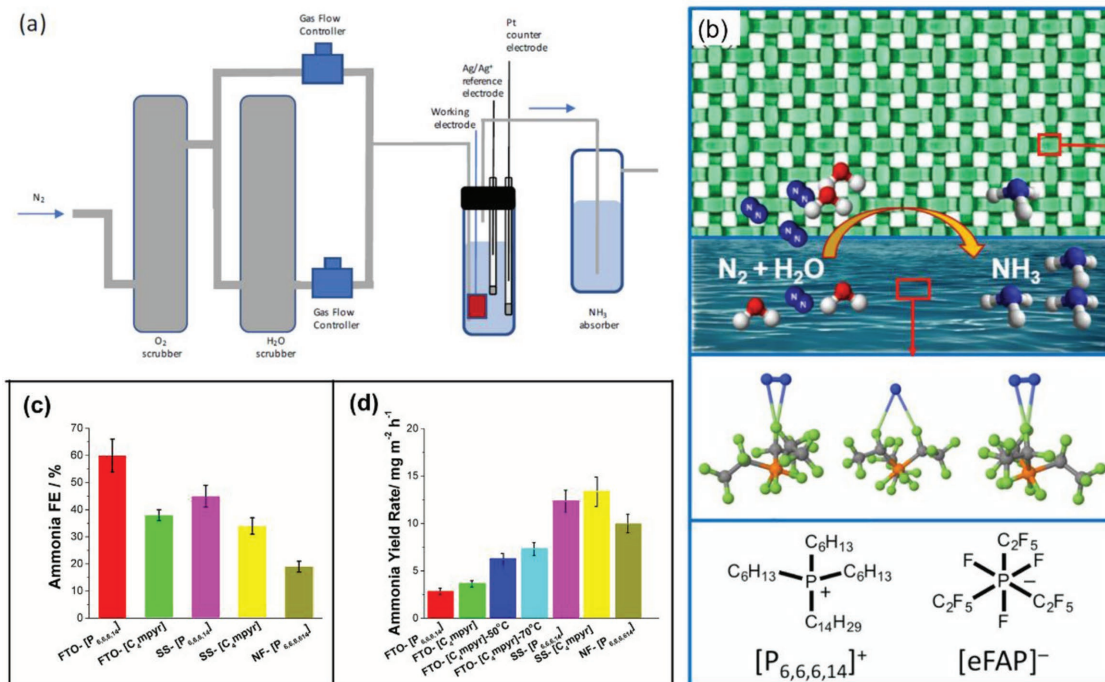


**Figure 13.** a) Schematic of an electrocatalytic NRR system with a single chamber cell using ionic liquids as electrolytes. b) NRR process on a Fe-stainless steel mesh electrode. c) The NH<sub>3</sub> Faradaic efficiency. d) The NH<sub>3</sub> production rate on different electrodes using N<sub>2</sub>-saturated ionic liquids at -0.8 V vs NHE. Reproduced with permission.<sup>[120]</sup> Copyright 2017, The Royal Society of Chemistry.

and the impact of the  $\text{NO}_x$  present in the gas stream was evaluated by control experiments. Additionally, to clarify the origin of the nitrogen in the ammonia produced,  $^{15}\text{N}_2$  reduction experiment was carried out and the ammonia was quantified by using a  $^1\text{H-NMR}$  measurement.

Apart from limiting the proton transfer rate by reducing the concentration of protons in the bulk solution, adding protection layers that can increase the barrier for proton transfer to the surface is possible to reduce the effective proton concentration near the surface without changing the number of proton donors in the bulk solution. The strategies for suppressing HER in rechargeable metal-based battery systems in aqueous media, such as the incorporation of bismuth or stannate additives to iron electrodes,<sup>[121,122]</sup> and the use of organo-sulfur compounds in alkaline electrolytes as steric hindrance,<sup>[123]</sup> may also shed light on suppressing HER in the electrochemical system for improving NRR selectivity. In fact, steric hindrance by ligand tethering was proposed to stabilize and protect key intermediates from intermolecular side reactions of molecular catalysts for NRR.<sup>[13]</sup> Moreover, the electronic flexibility of the ligand also contributed to the stabilization of different oxidation states of the metal active sites during catalysis. Similarly, it is reasonable to believe that surface tethering of the heterogeneous catalysts can as well help stabilizing key intermediates and metal active centers to boost NRR activity and selectivity.

Moreover, controlling the electron transfer rate at the interface of the electrode current collector and the catalyst,<sup>[124]</sup> or at the interface of the electrolyte and the catalyst,<sup>[125]</sup> may also help to suppress HER and facilitate  $\text{N}_2$  reduction. Note that limiting the electron transfer rate to suppress HER may come at the cost of reducing the efficiency of the system. Therefore, the balance between selectivity and efficiency should be considered for achieving optimal performance.

### 5.3. Avoiding HER by Decoupling $\text{N}_2$ Fixation and $\text{NH}_3$ Production

An alternative route for electrochemical  $\text{N}_2$  reduction is to utilize the spontaneous reaction of lithium metal with dinitrogen to form lithium nitrides at room temperature, which then reacts with proton donors to generate ammonia. This method was first applied to  $\text{NH}_3$  synthesis by Tsuneto et al. in the early 1990s.<sup>[126,127]</sup>  $\text{N}_2$  was reduced at  $-4.0$  V vs  $\text{Ag}/\text{AgCl}$  on different metal electrodes (Al, Ti, Mo, Fe, Co, Ni, Cu, Ag, etc.) in a solution of  $\text{LiClO}_4$  (0.20 M) in tetrahydrofuran/ethanol (99:1 v/v). The  $\text{Li}^+$  ions form metallic Li at the cathode and then turn to lithium nitride intermediates which react with the proton source to form  $\text{NH}_3$ . Hence, metal electrodes that readily alloy with Li give poor conversion efficiencies to  $\text{NH}_3$ . Both Ag and Ti afford the best CE of  $\approx 8\%$  for  $\text{NH}_3$  formation under 1 atm of  $\text{N}_2$ . A much higher CE of 48.7% was achieved under 50 atm of  $\text{N}_2$ .<sup>[126]</sup> The CE was found to rely on the type of cathode metal and the type and concentration of the proton source. Moreover,  $\text{NH}_3$  was even formed when air was used as the  $\text{N}_2$  source with a CE of 3.7%.<sup>[127]</sup> The reduced CE was presumably due to the side reaction of metallic Li with  $\text{O}_2$  in the air. Given that the presence of water was believed to inhibit  $\text{NH}_3$  formation, hydrophobic ionic liquids were used

as electrolyte with  $\text{LiClO}_4$  as the  $\text{Li}^+$  ion source in a study conducted by Pappenfus et al. using ethanol as the proton source and a Ni cathode.<sup>[128]</sup> A current efficiency of 3–5% (with a current density of  $2 \text{ mA cm}^{-2}$ ) was achieved at room temperature and atmospheric pressure. However, breakdown of the ionic liquid electrolyte was observed, resulting in serious stability issues.

A rechargeable lithium–nitrogen battery prototype has been demonstrated.<sup>[129]</sup> The battery system consists of a Li anode, a glass fiber separator, ether-based electrolyte, and a carbon cloth cathode (Figure 14a). The charging/discharging process corresponds to  $\text{N}_2$  evolution/fixation, respectively. The FE during  $\text{N}_2$  fixation increased from 32% (5 h) to a maximum value of 59% (7 h) and then reduced to 39% (9 h) in galvanostatic tests. In contrast, the FE was found to be up to 64% at 1.08 V after 5 h of potentiostatic testing. The incorporation of Ru or  $\text{ZrO}_2$  catalysts to a carbon cloth cathode improved both the stability of the Li– $\text{N}_2$  battery and the FE at 1.08 V. This promising research on nitrogen fixation batteries affords an advanced  $\text{N}_2/\text{Li}_3\text{N}$  cycle for reversible  $\text{N}_2$  fixation and future energy-storage system. More efforts should be made to further improve the stability of the Li– $\text{N}_2$  battery system and elucidate the underlying reaction mechanism. Lately, a lithium-mediated cycling process for  $\text{NH}_3$  synthesis from  $\text{N}_2$  and  $\text{H}_2\text{O}$  at ambient pressures has been reported, in which molten  $\text{LiOH}$  electrolysis, Li nitridation, and  $\text{Li}_3\text{N}$  hydrolysis were combined in a step-wise way (Figure 14b), enabling  $\text{NH}_3$  production with an initial overall current efficiency of 88.5%.<sup>[130]</sup> This electrochemical cycling strategy is capable of exceptional efficiency and selectivity compared to typical aqueous electrochemical approaches due to the ability to circumvent the otherwise competing and dominant  $\text{H}_2$  evolution reaction. However, this molten approach for  $\text{LiOH}$  electrolysis required high temperature, resulting in potential complexity during the separation of liquid Li from the molten salt system. Very recently, a hybrid electrolytic system that enables the deposition of Li under ambient temperature was reported.<sup>[131]</sup> A Li-ion conducting glass ceramic material was used to separate the aqueous side from the organic side where Li was deposited on a Ni substrate and then exposed to a  $\text{N}_2$  atmosphere for nitridation (Figure 14c). The  $\text{Li}_3\text{N}$  formed on Ni was then immersed in dilute sulfuric acid to trigger instantaneous formation of  $\text{NH}_4^+$ . Notably, the formation of a solid–electrolyte interface (SEI) layer during Li deposition can lead to the loss of active metallic Li, preventing Li from directly reacting with  $\text{N}_2$  at room temperature, thereby lowering the overall FE for  $\text{NH}_3$  formation. Hence, a high temperature ( $220$  °C) was chosen for Li deposition and nitridation, and the deposited Li was washed with 2-methyltetrahydrofuran before nitridation to inhibit side reactions between the metallic Li and the solvent. Finally, a maximum FE of 52.3% was obtained.

Considering that the nitridation properties of lithium metal are strongly affected by its surface, whereas the hydrolysis of lithium nitride is also dependent on the reaction rate and temperature,<sup>[132]</sup> further investigation to improve the performance of such a lithium-mediated system is requested. For instance, new strategies to minimize lithium-consuming side reactions at low temperatures are in demand for the system to operate under more benign conditions.

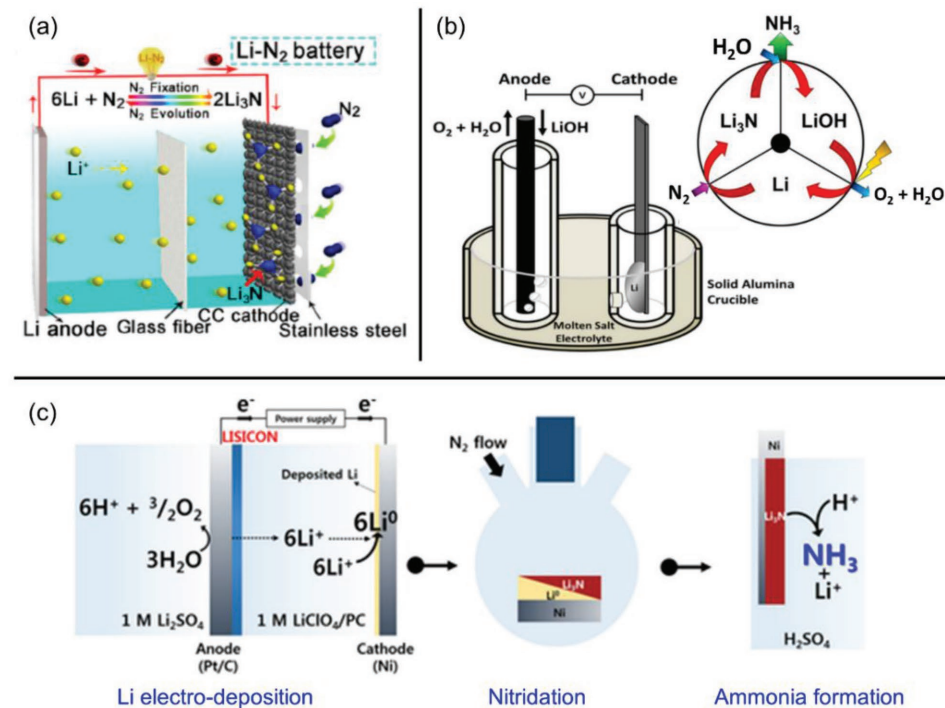


**Figure 14.** Different kinds of lithium-mediated systems for N<sub>2</sub> fixation and NH<sub>3</sub> formation under ambient conditions. a) Schematic structure of the reversible Li–N<sub>2</sub> battery. Reproduced with permission.<sup>[129]</sup> Copyright 2017, Elsevier Inc. b) Schematic cross section of the electrolysis cell for Li production and an illustration of the Li–Li<sub>3</sub>N–LiOH cycle. Reproduced with permission.<sup>[130]</sup> Copyright 2017, The Royal Society of Chemistry. c) Three-step Li-mediated synthesis of NH<sub>3</sub>. Reproduced with permission.<sup>[131]</sup> Copyright 2017, Wiley-VCH.

## 6. Methods for Determination of Ammonia

Methods for determining ammonia–nitrogen (NH<sub>3</sub>–N) in aqueous media after NRR electrochemical measurements have been proposed, including ion chromatography methods,<sup>[135,134]</sup> spectrophotometric/colorimetric methods,<sup>[135,136]</sup> ion-selective electrode (ISE) methods,<sup>[137]</sup> and fluorescence methods.<sup>[138]</sup> Among them, ion chromatography, though requires expensive and complex instrumentation, has the advantages of high sensitivity, good reproducibility, simultaneous determination of multiple ions in a short time, and the possibility of using different detectors (conductometric, fluorimetric, UV-vis, etc.).<sup>[139]</sup> For the determination of ammonium ions (NH<sub>4</sub><sup>+</sup>), the main interference is the overlapping of the Na<sup>+</sup> peak and the NH<sub>4</sub><sup>+</sup> peak.<sup>[140]</sup> This problem can be tackled by using a column-switching technique or by applying the appropriate columns and eluents that enable facile determination of trace-level cations even in a high-ionic-strength matrix.<sup>[133,134,141]</sup>

The spectrophotometric methods, also known as the colorimetric methods, are widely used for ammonia nitrogen detection in freshwater/seawater/wastewater. Among them, the indophenol blue method based on the Bethelot reaction, in which ammonia reacts with phenol and hypochlorite in alkaline solution, is commonly employed as a standard reference method for determining low-concentration ammonia nitrogen (0–0.6 mg NH<sub>3</sub>–N L<sup>-1</sup>).<sup>[142]</sup> The reaction is catalyzed by sodium nitroprusside for intensified color development. However, the blue color of indophenol sometimes is replaced by a yellow or green color, resulting in unreliable results.<sup>[135]</sup> The salicylate

method based on a modified Bethelot reaction is more widely used than the phenate method nowadays, in which sodium salicylate is substituted for phenol to eliminate the formation of toxic and highly volatile reagents.<sup>[143]</sup> To achieve a sensitivity comparable to that in the case of phenol, large amounts of reagents are used in the salicylate method. The color development of the salicylate method is more stable than the phenate method.<sup>[135]</sup> The Nessler's reagent method, in which ammonia reacts with the Nessler's reagent (alkaline solution of mercuric potassium iodide, K<sub>2</sub>HgI<sub>4</sub>) to give a color complex, is less time consuming and requires less reagents than the standard salicylate method. Pretreatments are requested to eliminate the interfering effect of metal ions, residual chlorine, sulfides, and organics. For instance, Rochelle salt (KNaC<sub>4</sub>H<sub>4</sub>O<sub>6</sub>·4H<sub>2</sub>O) solution is usually added to remove residual hardness cations that might react with the Nessler's reagent.<sup>[135]</sup> Note that the Nessler's reagent contains mercury, which is very toxic and dangerous to the environment, causing disposal problems. It is worth noting that commercial products based on the colorimetric methods such as ammonia colorimetric assay kits have been used for much simpler procedures,<sup>[48,124]</sup> and ammonia test strips for quick and simple detection.<sup>[55]</sup>

There are two types of ISE for sensing ammonia nitrogen concentration. One is the ammonia-selective electrode that consists of a pH-sensing electrode, an internal reference electrode, and a hydrophobic ammonia permeable membrane. When a strong base is added, ammonium ions in the sample solution turn to ammonia gas. The gas then diffuses through the membrane and causes a potential difference that can be measured by a high

impedance voltmeter. The measured potential, in accordance with the Nernst equation, is proportional to the ammonia/ammonium concentration in the solution. The other is the ammonium ion-sensing electrode that has a polyvinylchloride (PVC) membrane containing an ammonium-ion carrier. The sample is acidified to convert all  $\text{NH}_3$  to  $\text{NH}_4^+$  for measurement. The ion-selective method is much more convenient and rapid than the spectrophotometric methods, with much larger detection range ( $0.03\text{--}1400 \text{ mg NH}_3\text{-N L}^{-1}$ ) and possibility for continuous monitoring.<sup>[144]</sup> However, the precision, accuracy, repeatability, and stability for ammonia nitrogen at low concentration (e.g.,  $<0.5 \text{ mg L}^{-1}$ ) is not as good as those at higher concentration of ammonia nitrogen. It is necessary to ensure good sealing of the standard solution and the sample before measuring, and use containers with small opening to prevent the escape of ammonia when measuring. It is worth noting that for solutions with low ammonia/ammonium concentration but high in total ionic strength, a calibration solution with a background composition similar to the sample should be used for accurate measurements. Samples and standard solutions should be at the same temperature. Interferences including volatile amines, ionic strength of the solution, metallic ions that complex ammonia, and pH effect should be considered. To inhibit the formation of some common metal complexes in the sample and to avoid the pH effect, an ionic strength adjustor solution is often added to the sample. The total ammonia–nitrogen measured is strongly affected by the presence of sodium and potassium ions in the solution for the  $\text{NH}_4^+$ -sensing electrode.<sup>[135,145]</sup> Commercial ion-selective electrodes are available, such as the Orion 9512HPBNWP  $\text{NH}_3$  electrode and the Radiometer Analytical ISE25NH4-9  $\text{NH}_4^+$  electrode.

In terms of overall accuracy and precision, neither the Nessler's reagent method or the ion-selective electrode method was superior to the standard indophenol blue method. However, the routine manual spectrophotometric methods do not excel at determining ammonia at nanomolar concentrations. In contrast, the fluorometric method based on the reaction of ammonium with *o*-phthalodialdehyde (OPA) and sulfite is of high sensitivity. This method is often combined with flow analysis for the determination of ammonium at nanomolar concentrations in natural waters,<sup>[146–148]</sup> yet suffering from interferences such as amines and amino acids.<sup>[138]</sup> The OPA fluorometric method is not suitable for determining ammonium at micromolar and millimolar level, because too much dilution to fit the linearity range of the method leads to serious errors. In recent years, flow injection techniques combined with spectrophotometry have been widely used for online determination of ultratrace ammonium in water samples. For instance, a detection limit of  $3.6 \text{ nmol L}^{-1}$  and a linearity of  $10\text{--}500 \text{ nmol L}^{-1}$  were achieved by an automatic indophenol blue spectrophotometric method combined with flow injection analysis using a long-path liquid waveguide capillary cell.<sup>[149]</sup> The upper limit can be extended to  $30 \mu\text{mol L}^{-1}$  by lowering the reaction temperature or choosing a less sensitive detection wavelength.

A comparison of different ammonia determination methods is given in Table 1. There is an urgent demand for developing more selective and more accurate ammonia determination methods at nanomolar concentrations, as well as continuous monitoring and rapid on-site determination for NRR tests. Moreover, a combination of different methods can be more reliable and more convincing.

**Table 1.** A comparison of different ammonia determination methods.

Method (including commercial products)	Detection range [mg $\text{NH}_3\text{-N L}^{-1}$ ] <sup>[Ref.]</sup>	Wavelength and pH	Interfering factors and other issues
Ion chromatography	0.02–40 <sup>[133]</sup>	–	Selected amino acids, aliphatic amines, and some metal ions, $\text{Na}^+$
Phenate method	0.01–2.0 <sup>[135]</sup>	630–640 nm pH > 11	$\text{Mg}^{2+}, \text{Ca}^{2+}$ complex, occasional color development error, time consuming, toxicity
Salicylate method	0.01–1.0 <sup>[135]</sup>	667–697 nm pH > 11	pH effect, time consuming, low toxicity
Nessler's reagent method	0.025–5.0 <sup>[135]</sup>	410–425 nm pH > 11	Metallic ions, chlorine, sulfides, and organics interfering, stability issue, toxicity
Ammonia colorimetric assay kit (BioVision K370)	<0.28	≈570 nm	Check the user manual
Ammonia colorimetric assay Kit (BioVision K470)	<0.14	≈670 nm	Check the user manual
Ammonia (nitrogen) test strips (Hach 2755325)	0–6.0	–	Check the user manual
Hach Nessler kit, Model NI-8	0–3.0	–	Check the user manual
Ammonia-ion selective electrode (AISE) (Hach)	0.067–17 000	pH > 11 and Ionic strength adjustor (ISA)	Volatile amines, ionic strength, and metallic ions interfering, less precise and accurate at low ammonia concentration, escape of ammonia gas
Ammonia electrode (Orion 9512HPBNWP)	0.01–17 000	pH > 11 and ISA	
$\text{NH}_4^+$ selective electrode (Radiometer Analytical ISE25NH4-9)	0.06–20 000	pH > 11 and ISA	$\text{Na}^+, \text{K}^+$ interfering for $\text{NH}_4^+$ electrode, other issues are the same as above AISE
OPA fluorometric method coupled with flow injection	$1.0 \times 10^{-4} \text{--} 2.8 \times 10^{-3}$ <sup>[147]</sup>	–	Complex instrument
Indophenol blue method coupled with flow injection	$1.4 \times 10^{-4} \text{--} 0.42$ <sup>[149]</sup>	≈690 nm	Complex instrument

## 7. Conclusions and Outlook

Recent theoretical studies that provide material screening and catalyst structure design guidance for electrochemical nitrogen reduction and ammonia formation under ambient conditions have been discussed. Rational design of catalysts along with favorable electrochemical cell configurations has been presented, and strategies for constructing an active, selective, and efficient electrochemical system have been provided. Moreover, ammonia determination methods were evaluated. Rapid and accurate measurements are in great demand. A performance summary of various NRR catalysts along with the cell configuration and ammonia determination method is given in **Table 2**. In spite of the enormous progress made in the past years, it is still very challenging for designing effective NRR catalysts and constructing excellent NRR electrochemical systems capable of operating under ambient conditions. Problems including high overpotential, low NH<sub>3</sub> yield, poor NH<sub>3</sub> selectivity and efficiency, as well as unsatisfied catalyst stability call for substantial further research efforts in to this field. To realize electrochemical NRR to a more practical level, the following aspects demand to be scrutinized:

- i) *Better Understanding of the NRR Mechanism to Accelerate Further Development in This Field*: Theoretical calculations and computational methods have made it feasible to investigate electrocatalysts at the atomic level. Nevertheless, further improvements of the computational methods and models for NRR at heterogeneous catalyst surfaces are highly demanded. Computational studies on heterogeneous electrocatalysis typically employ the so-called computational hydrogen electrode (CHE) methodology that has been successful in predicting the thermodynamics of CPET steps. However, the CHE methodology cannot account for SPET pathways. Therefore, theoretical methods to describe possible SPET pathways are requested. Moreover, the vacuum-calculated adsorption energies are not sufficient in electrochemical reactions under operating conditions. Guiding principles and predictive models capturing medium effects (e.g., pH, the proton sources, and the buffer cations/anions) and surface reconstruction of catalysts under electrochemical conditions are desirable. Furthermore, both theoretical calculations and experiments should be combined to provide deeper insights into the reaction interfaces between the electrocatalysts and the electrolytes.
- ii) *Rational Design of the Catalysts and the Electrochemical System*: The catalytic activity and selectivity toward NH<sub>3</sub> formation of almost all current NRR electrocatalysts in aqueous systems are extremely low mainly due to the dominating HER that shuttles electrons and protons to form hydrogen. Therefore, strategies to suppress or even circumvent HER are requested to significantly improve the catalytic activity and selectivity. Crystal facet engineering, defect engineering, strain engineering, cation/anion regulating, heteroatom doping, reticular chemistry, surface tethering, and electrode/catalyst/electrolyte interface engineering are highly expected to suppress HER and boost NRR. The breaking of scaling relations for electrocatalytic NRR is important to reduce the overpotentials and achieve better performance. Both the surface properties and the electrochemical environments can substantially change the overpotentials of electrocatalytic reactions.<sup>[22]</sup> Successful examples in the field of CO<sub>2</sub>ERR,<sup>[117]</sup> as well as effective catalyst design for high-temperature N<sub>2</sub> activation and NH<sub>3</sub> synthesis can be helpful.<sup>[43,150]</sup> Using nonaqueous proton donor is another possible way to break the scaling between the limiting potential and the binding energies.<sup>[151]</sup> On the other hand, approaches to decoupling the reduction of N<sub>2</sub> from subsequent protonation to NH<sub>3</sub> to completely circumvent HER should also be further investigated. The grand challenge does not lie solely in catalyst design, but rather in implementing the catalyst within suitable electrochemical system, so as to control the interplay between activity, selectivity, efficiency, and stability. Currently, the activity and selectivity issues are more urgent to be tackled. For future research activities, the efficiency and stability issues should be considered more seriously when exploring effective catalysts and constructing an excellent electrochemical system. Theoretical studies indicated that some transition metal nitrides decomposed at certain potentials upon electrochemical tests.<sup>[60,61]</sup> The NH<sub>3</sub> yields and the NH<sub>3</sub> Faradaic efficiency apparently decreased experimentally after certain time.<sup>[50,81]</sup> The active sites can be poisoned or deactivated during long-term electrochemical tests. Therefore, durability tests are highly requested for improving the commercial viability of the electrochemical system.
- iii) *Clarification of the Origin of Nitrogen in the Ammonia Generated*: Importantly, N<sub>2</sub> isotope labeling experiments are requested to clarify the origin of the nitrogen in the ammonia/ammonium generated in the electrochemical system, especially when nitrogen atoms were presented in the electrode/catalyst/electrolyte. Experiments must be carried out to prove that nitrogen is coming from the molecular dinitrogen applied to the system, instead of other sources of activated nitrogen generated by nitrogen-containing compounds being present either in the catalysts or in the electrolytes. The origin of nitrogen can be convincingly proved by using isotopically labeled <sup>15</sup>N<sub>2</sub> and be quantified using mass spectroscopy, NMR, or IR spectroscopy. For instance, the <sup>1</sup>H NMR signal of <sup>15</sup>NH<sub>4</sub><sup>+</sup> and the Fourier-transform infrared spectroscopy (FTIR) spectra for isotopically labeled ammonia indicatively synthesized from <sup>15</sup>N<sub>2</sub> have been used in previous studies.<sup>[120,130]</sup>
- iv) *Standard Protocols for the Electrochemical NRR Measurement Techniques*: Though no complete consensus has been reached on the mandated, fixed procedures for implementing NRR measurements, there are some strict instructions for further research activities in this field. In terms of the catalysts for NRR, if the catalyst itself contains N atoms, then <sup>15</sup>N isotopic measurements are needed to clarify that the N atoms in the generated NH<sub>3</sub> are indeed originated from the applied N<sub>2</sub>. In contrast, if the catalyst itself does not contain N atoms in principle, whereas nitrogen-containing reagents or surfactants are employed during the synthetic processes, then clarification of the origin of N atoms in the generated NH<sub>3</sub> is still requested. One way to rule out such misleading factors is to avoid using nitrogen-containing chemicals during the synthetic processes and avoid contamination during the washing and drying of the catalyst materials. In terms of the electrolytes and the electrode (current collector, gas diffusion

**Table 2.** A brief summary of the representative experimental studies on N<sub>2</sub> electroreduction and NH<sub>3</sub> formation using various heterogeneous catalysts.

Catalyst <sup>[Ref.]</sup>	Cell type, electrolyte	Conditions [all at 1 atm]	Methods for ammonia determination	Ammonia formation rate [ $\mu\text{g h}^{-1} \text{cm}^{-2}$ ]	Faradaic efficiency [%]
Ru/C <sup>[83]</sup>	PEM-type cell, 2.0 M KOH	90 °C	Phenate method and ion Chromatography	0.25, at -0.96 V vs Ag/AgCl	0.92
		20 °C		0.21, at -1.10 V vs Ag/AgCl	0.28
30 wt% Pt/C <sup>[79]</sup>	Back-to-back cell, 0.50 M H <sub>2</sub> SO <sub>4</sub>	Room temperature (RT)	Nessler's reagent method	69.8, at 1.6 V cell voltage	0.5
30 wt% Pt/C <sup>[80]</sup>	Back-to-back cell, Li <sup>+</sup> /H <sup>+</sup> /NH <sub>4</sub> <sup>+</sup> mixed electrolyte	80 °C	Nessler's reagent method	47.2, at 1.2 V cell voltage	0.83
Ru/Ti <sup>[90]</sup>	single chamber cell, 0.50 M H <sub>2</sub> SO <sub>4</sub>	30 °C	Salicylate method	7.31, at 2 mA cm <sup>-2</sup>	N/A
Rh/Ti <sup>[90]</sup>	single chamber cell, 0.50 M H <sub>2</sub> SO <sub>4</sub>	30 °C	Salicylate method	0.918, at 2 mA cm <sup>-2</sup>	N/A
Pt <sup>[119]</sup>	Back-to-back cell, 6 M KOH/polymer gel	30 °C	Indophenol blue method	0.191 at 0.5 V cell voltage	0.01
Ir <sup>[119]</sup>	Back-to-back cell, 6 M KOH/polymer gel	60 °C	Indophenol blue method	0.130 at 0.25 V cell voltage	0.1
Ru nanosheets <sup>[87]</sup>	H-type cell, 0.10 M KOH	RT	Indophenol blue method	23.88 $\mu\text{g h}^{-1} \text{mg}^{-1}_{\text{cat}}$ at -0.2 V vs RHE	0.217
Au nanorods <sup>[48]</sup>	H-type cell, 0.10 M KOH	RT	NH <sub>3</sub> assay kit and Nessler's reagent method	1.648, at -0.2 V vs RHE	4.0
Au/TiO <sub>2</sub> <sup>[49]</sup>	H-type cell, 0.10 M KOH	RT	Salicylate method	21.4 $\mu\text{g h}^{-1} \text{mg}^{-1}_{\text{cat}}$ at -0.2 V vs RHE	8.11
Au–CeO <sub>x</sub> /RGO <sup>[85]</sup>	H-type cell, 0.10 M KOH	RT	Salicylate method	8.3 $\mu\text{g h}^{-1} \text{mg}^{-1}_{\text{cat}}$ at -0.2 V vs RHE	10.1
Fe plate <sup>[73]</sup>	H-type cell, 6.0 M KOH	45 °C	Indophenol blue method	2.8 × 10 <sup>-3</sup> , at -1.07 V vs SCE	1
Fe-phthalocyanine <sup>[74]</sup>	H-type cell, 1.0 M KOH	25 °C	Nessler's reagent method	10.0–26.8 (within 20 min) at -47.8 mA cm <sup>-2</sup>	0.12–0.35
Fe, FeNi, Ni <sup>[81]</sup>	N/A basic electrolyte	50 °C	N/A	0.067–0.191, at 1.2 V cell voltage	1.1–41
Fe on stainless steel mesh <sup>[120]</sup>	H-type cell, Ionic liquids with trace amounts of water	RT	Indophenol blue method	1.4, at -0.8 V vs NHE (with [C4mpyr][eFAP])	30
Porous Ni <sup>[91]</sup>	single chamber cell, 2-propanol/H <sub>2</sub> SO <sub>4</sub>	RT	Indophenol blue method	0.942, at 0.5 mA cm <sup>-2</sup>	0.89
Ni wire <sup>[92]</sup>	H-type cell, Cathode: EDA/LiCl, Anode: 0.050 M H <sub>2</sub> SO <sub>4</sub>	RT	N/A	32.8, at 1.8 V cell voltage	17.2
Mo nanofilm <sup>[93]</sup>	H-type cell 0.010 M H <sub>2</sub> SO <sub>4</sub>	RT	Salicylate method	1.89, at -0.49 V vs RHE	0.72, at -0.29 V vs RHE
MOF (Fe) <sup>[114]</sup>	PEM-type cell, 2.0 M KOH	90 °C	Nessler's reagent method	129.74, at 1.2 V cell voltage	1.43
Fe <sub>2</sub> O <sub>3</sub> –CNT <sup>[84]</sup>	PEM-type cell 2.0 M NaHCO <sub>3</sub>	RT	Salicylate method and ion-selective electrode	0.22, at -2.0 V vs Ag/AgCl	0.15 at -1.0 V vs Ag/AgCl
30 wt% Fe <sub>2</sub> O <sub>3</sub> –CNT <sup>[85]</sup>	PEM-type cell 0.50 M KOH	RT	Salicylate method	0.649, at -2.0 V vs Ag/AgCl	0.164
$\alpha$ -Fe <sub>2</sub> O <sub>3</sub> /CNT, our work	PEM-type cell 0.10 M KOH	25 °C	Nessler's reagent method	0.459, at -0.9 V vs Ag/AgCl	6.0
$\gamma$ Fe <sub>2</sub> O <sub>3</sub> <sup>[82]</sup>	Back-to-back cell with AEM, 0.50 M KOH	65 °C	Indophenol blue method and Nessler's reagent method	0.95, at 1.6 V cell voltage	0.044
	Single chamber cell, 0.10 M KOH			0.74, at 0 V vs RHE	1.96

**Table 2.** Continued.

Catalyst <sup>[Ref.]</sup>	Cell type, electrolyte	Conditions [all at 1 atm]	Methods for ammonia determination	Ammonia formation rate [ $\mu\text{g h}^{-1}\text{cm}^{-2}$ ]	Faradaic efficiency [%]
ZnS <sup>[75]</sup>	single chamber cell, 1.0 M KOH	25 °C	Nessler's reagent method	345.96, at -1.0 V vs RHE	0.964
ZnSe <sup>[75]</sup>	single chamber cell, 1.0 M KOH	25 °C	Nessler's reagent method	393.87, at -1.0 V vs RHE	1.29
SmFe <sub>0.7</sub> Cu <sub>0.1</sub> Ni <sub>0.2</sub> O <sub>3</sub> <sup>[77]</sup>	Back-to-back cell	80 °C	Nessler's reagent method	691.56, at 3.5 mA cm <sup>-2</sup>	90.4
Sm <sub>1.5</sub> Sr <sub>0.5</sub> NiO <sub>4</sub> <sup>[78]</sup>	Back-to-back cell	80 °C	Nessler's reagent method	642.6, at 2.5 V cell voltage	N/A
Polyaniline <sup>[88]</sup>	single chamber cell, methanol/LiClO <sub>4</sub> /H <sub>2</sub> SO <sub>4</sub>	25 °C	Indophenol blue method	3.82, at -0.12 V vs NHE	2.0
PEBCD/C <sup>[86]</sup>	H-type cell, 0.50 M Li <sub>2</sub> SO <sub>4</sub>	25 °C 40 °C	Nessler's reagent method	1.58, at -0.5 V vs RHE 4.33, at -0.5 V vs RHE	2.85 4.87
Bi <sub>4</sub> V <sub>2</sub> O <sub>11</sub> /CeO <sub>x</sub> <sup>[94]</sup>	H-type cell, HCl, pH = 1	RT	Indophenol blue method	23.21 $\mu\text{g h}^{-1}\text{mg}^{-1}_{\text{cat}}$ at -0.2 V vs RHE	10.16
N-doped carbon <sup>[95]</sup>	H-type cell, 0.05 M H <sub>2</sub> SO <sub>4</sub>	RT	Nessler's reagent method	11.76 at -0.9 V vs RHE	1.42

layer, etc.), if these parts contain N species, clarification of the origin of N atoms in the generated NH<sub>3</sub> is also requested. To accelerate the experimental material screening for efficient NRR electrocatalysts, there is an urgent need for developing more accurate ammonia determination method at nanomolar concentrations, as well as continuous monitoring and rapid on-site measurements. Importantly, since the spectrophotometric methods and the ion chromatography methods allow for the detection of ammonia down to the ppm or even ppb level, contamination of ammonia on the ppm level will result in erroneous conclusions. It is therefore recommended that the electrochemical system as well as the environment where the measurements are carried out should be checked for possible ammonia contamination.

v) *Advanced Characterization Techniques for NRR Electrocatalysts in the Electrochemical System:* In recent years, *in situ* and *operando* studies have played a crucial role in describing the local and electronic structures of electrocatalyst in its functional form and under operating conditions.<sup>[152]</sup> For instance, phase changes associated with ORR and OER activities upon applied potentials have been observed by using *in situ* X-ray absorption near edge structure and extended X-ray absorption fine structure.<sup>[153]</sup> In another case, real-time attenuated total reflection, surface-enhanced infrared absorption spectroscopy (SEIRAS), isotopic labeling, and electrochemical techniques were combined to investigate the CO<sub>2</sub>RR mechanisms on a Cu thin-film electrode, allowing for direct observation of reaction intermediates and understanding the role of the electrolyte in the reaction.<sup>[154]</sup> Similarly, the adsorbed species on its surface during NRR under operating conditions demand to be scrutinized by *in situ* and *operando* techniques for better understanding of the catalytic reaction mechanisms. For instance, SEIRAS was recently employed to study the NRR mechanisms on a Au thin film.<sup>[155]</sup> Adsorbed N<sub>2</sub>H<sub>y</sub> species were detected, indicating an associative reaction mechanism on Au surfaces. Moreover, possible dynamic changes of the catalyst surface as well as the role of the electrolyte during the NRR process are to be discovered in the near future by employing advanced *in situ* and *operando* techniques.

vi) *Development of Electrochemical Methods for NRR:* So far, there are very limited reports on the Tafel plots of NRR. Besides, rotating disk electrode and rotating ring disk electrode measurements are desirable for exploring the electrode kinetics and the electron transfer behaviors with the applied potential which is commonly used in electrocatalysis such as ORR, OER, and HER.

In summary, the great progress in the field of NRR has confirmed the possibility of electrochemical reduction of N<sub>2</sub> to NH<sub>3</sub> on heterogeneous surfaces under ambient conditions. Despite the grand challenges ahead, we believed that a combination of theoretical and experimental investigations, together with the use of *in situ/operando* characterization techniques and online fast and accurate ammonia/ammonium nitrogen measurements will further push the development of more active, more selective, more efficient, and more stable heterogeneous electrocatalysts for N<sub>2</sub> reduction and NH<sub>3</sub> formation in the near future.

## Acknowledgements

This work was supported by National Key Research and Development Program (2016YFA0202500), National Natural Scientific Foundation of China (Grant Nos. 21676160 and 21706146), and China Postdoctoral Science Foundation (2016M600097). The authors thank Hao-Fan Wang, Bin Wang, Bo-Quan Li, Ling Zhong, and Xiaomeng Liu for helpful discussions.

## Conflict of Interest

The authors declare no conflict of interest.

## Keywords

electrocatalysis, electrocatalytic reduction of dinitrogen, electrochemical ammonia synthesis, nitrogen reduction reaction, sustainable chemistry

Received: February 2, 2018

Revised: March 16, 2018

Published online: May 21, 2018

- [1] Z. W. Seh, J. Kibsgaard, C. F. Dickens, I. Chorkendorff, J. K. Nørskov, T. F. Jaramillo, *Science* **2017**, *355*, 146.
- [2] R. Schlögl, *Handbook of Heterogeneous Catalysis*, Wiley-VCH, Weinheim, Germany **2008**.
- [3] I. A. Amar, R. Lan, C. T. G. Petit, S. Tao, *J. Solid State Electrochem.* **2011**, *15*, 1845.
- [4] S. Giddey, S. P. S. Badwal, A. Kulkarni, *Int. J. Hydrogen Energy* **2013**, *38*, 14576.
- [5] J. N. Galloway, A. R. Townsend, J. W. Erisman, M. Bekunda, Z. Cai, J. R. Freney, L. A. Martinelli, S. P. Seitzinger, M. A. Sutton, *Science* **2008**, *320*, 889.
- [6] C. Zamfirescu, I. Dincer, *J. Power Sources* **2008**, *185*, 459.
- [7] H. Liu, *Chin. J. Catal.* **2014**, *35*, 1619.
- [8] Y. Tanabe, Y. Nishibayashi, *Coord. Chem. Rev.* **2013**, *257*, 2551.
- [9] C. J. M. van der Ham, M. T. M. Koper, D. G. H. Hetterscheid, *Chem. Soc. Rev.* **2014**, *43*, 5183.
- [10] R. R. Eady, *Chem. Rev.* **1996**, *96*, 3013.
- [11] B. K. Burgess, D. J. Lowe, *Chem. Rev.* **1996**, *96*, 2983.
- [12] Y. Nishibayashi, *Inorg. Chem.* **2015**, *54*, 9234.
- [13] J. Rittle, J. C. Peters, *J. Am. Chem. Soc.* **2016**, *138*, 4243.
- [14] C. X. Guo, J. Ran, A. Vasileff, S. Qiao, *Energy Environ. Sci.* **2018**, *11*, 45.
- [15] C. S. Diercks, Y. Liu, K. E. Cordova, O. M. Yaghi, *Nat. Mater.* **2018**, *17*, 301.
- [16] T. H. Rod, A. Logadottir, J. K. Nørskov, *J. Chem. Phys.* **2000**, *112*, 5343.
- [17] A. R. Singh, B. A. Rohr, J. A. Schwalbe, M. Cargnello, K. Chan, T. F. Jaramillo, I. Chorkendorff, J. K. Nørskov, *ACS Catal.* **2017**, *7*, 706.
- [18] M. A. Shipman, M. D. Symes, *Catal. Today* **2017**, *286*, 57.
- [19] V. Kyriakou, I. Garagounis, E. Vasileiou, A. Vourros, M. Stoukides, *Catal. Today* **2017**, *286*, 2.
- [20] X. Guo, Y. Zhu, T. Ma, *J. Energy Chem.* **2017**, *26*, 1107.
- [21] N. Cao, G. Zheng, *Nano Res.* **2018**, <https://doi.org/10.1007/s12274-018-1987-y>.
- [22] C. Tang, H.-F. Wang, Q. Zhang, *Acc. Chem. Res.* **2018**, *51*, 881.
- [23] A. E. Shilov, *Russ. Chem. Bull.* **2003**, *52*, 2555.
- [24] H.-P. Jia, E. A. Quadrelli, *Chem. Soc. Rev.* **2014**, *43*, 547.
- [25] C.-G. Zhan, J. A. Nichols, D. A. Dixon, *J. Phys. Chem. A* **2003**, *107*, 4184.
- [26] T. A. Bazhenova, A. E. Shilov, *Coord. Chem. Rev.* **1995**, *144*, 69.
- [27] S. G. Bratsch, *J. Phys. Chem. Ref. Data* **1989**, *18*, 1.
- [28] G. Jones, T. Bligaard, F. Abild-Pedersen, J. K. Nørskov, *J. Phys.: Condens. Matter* **2008**, *20*, 064239.
- [29] I. C. Man, H.-Y. Su, F. Calle-Vallejo, H. A. Hansen, J. I. Martínez, N. G. Inoglu, J. Kitchin, T. F. Jaramillo, J. K. Nørskov, J. Rossmeisl, *ChemCatChem* **2011**, *3*, 1159.
- [30] M. T. M. Koper, *Chem. Sci.* **2013**, *4*, 2710.
- [31] I. Katsounaros, T. Chen, A. A. Gewirth, N. M. Markovic, M. T. M. Koper, *J. Phys. Chem. Lett.* **2016**, *7*, 387.
- [32] A. J. Gottle, M. T. M. Koper, *Chem. Sci.* **2017**, *8*, 458.
- [33] C. V. S. Kumar, V. Subramanian, *Phys. Chem. Chem. Phys.* **2017**, *19*, 15377.
- [34] Y. Abghoui, E. Skúlason, *Catal. Today* **2017**, *286*, 69.
- [35] A. J. Medford, A. Vojvodic, J. S. Hummelshøj, J. Voss, F. Abild-Pedersen, F. Studt, T. Bligaard, A. Nilsson, J. K. Nørskov, *J. Catal.* **2015**, *328*, 36.
- [36] A. Logadottir, T. H. Rod, J. K. Nørskov, B. Hammer, S. Dahl, C. J. H. Jacobsen, *J. Catal.* **2001**, *197*, 229.
- [37] T. Bligaard, J. K. Nørskov, S. Dahl, J. Matthiesen, C. H. Christensen, J. Sehested, *J. Catal.* **2004**, *224*, 206.
- [38] F. Abild-Pedersen, J. Greeley, F. Studt, J. Rossmeisl, T. R. Munter, P. G. Moses, E. Skúlason, T. Bligaard, J. K. Nørskov, *Phys. Rev. Lett.* **2007**, *99*, 016105.
- [39] S. Wang, V. Petzold, V. Tripkovic, J. Kleis, J. G. Howalt, E. Skúlason, E. M. Fernandez, B. Hvolbaek, G. Jones, A. Toftlund, H. Falsig, M. Bjørketun, F. Studt, F. Abild-Pedersen, J. Rossmeisl, J. K. Nørskov, T. Bligaard, *Phys. Chem. Chem. Phys.* **2011**, *13*, 20760.
- [40] E. Skúlason, T. Bligaard, S. Guðmundsdóttir, F. Studt, J. Rossmeisl, F. Abild-Pedersen, T. Vegge, H. Jonsson, J. K. Nørskov, *Phys. Chem. Chem. Phys.* **2012**, *14*, 1235.
- [41] J. G. Howalt, T. Bligaard, J. Rossmeisl, T. Vegge, *Phys. Chem. Chem. Phys.* **2013**, *15*, 7785.
- [42] M. M. Montemore, J. W. Medlin, *Catal. Sci. Technol.* **2014**, *4*, 3748.
- [43] P. Wang, F. Chang, W. Gao, J. Guo, G. Wu, T. He, P. Chen, *Nat. Chem.* **2017**, *9*, 64.
- [44] J. G. Howalt, T. Vegge, *Beilstein J. Nanotechnol.* **2014**, *5*, 111.
- [45] A. L. Garden, E. Skúlason, *J. Phys. Chem. C* **2015**, *119*, 26554.
- [46] S. Back, Y. Jung, *Phys. Chem. Chem. Phys.* **2016**, *18*, 9161.
- [47] A. Ishikawa, T. Doi, H. Nakai, *J. Catal.* **2018**, *357*, 213.
- [48] D. Bao, Q. Zhang, F.-L. Meng, H.-X. Zhong, M.-M. Shi, Y. Zhang, J.-M. Yan, Q. Jiang, X.-B. Zhang, *Adv. Mater.* **2017**, *29*, 1604799.
- [49] M.-M. Shi, D. Bao, B.-R. Wulan, Y.-H. Li, Y.-F. Zhang, J.-M. Yan, Q. Jiang, *Adv. Mater.* **2017**, *29*, 1606550.
- [50] S.-J. Li, D. Bao, M.-M. Shi, B.-R. Wulan, J.-M. Yan, Q. Jiang, *Adv. Mater.* **2017**, *29*, 1700001.
- [51] J. H. Montoya, C. Tsai, A. Vojvodic, J. K. Nørskov, *ChemSusChem* **2015**, *8*, 2180.
- [52] W. Yu, M. D. Porosoff, J. G. Chen, *Chem. Rev.* **2012**, *112*, 5780.
- [53] J. L. C. Fajín, M. N. D. S. Cordeiro, J. R. B. Gomes, *Appl. Catal., B* **2017**, *218*, 199.
- [54] X.-L. Ma, J.-C. Liu, H. Xiao, J. Li, *J. Am. Chem. Soc.* **2018**, *140*, 46.
- [55] S. Licht, B. Cui, B. Wang, F.-F. Li, J. Lau, S. Liu, *Science* **2014**, *345*, 637.
- [56] M.-T. Nguyen, N. Seriani, R. Gebauer, *Phys. Chem. Chem. Phys.* **2015**, *17*, 14317.
- [57] A. B. Höskuldsson, Y. Abghoui, A. B. Gunnarsdóttir, E. Skúlason, *ACS Sustainable Chem. Eng.* **2017**, *5*, 10327.
- [58] Y. Abghoui, A. L. Garden, V. F. Hlynsson, S. Bjørgvinssdóttir, H. Olafsdóttir, E. Skúlason, *Phys. Chem. Chem. Phys.* **2015**, *17*, 4909.
- [59] Y. Abghoui, E. Skúlason, *Procedia Computer Sci.* **2015**, *51*, 1897.
- [60] Y. Abghoui, A. L. Garden, J. G. Howalt, T. Vegge, E. Skúlason, *ACS Catal.* **2016**, *6*, 635.
- [61] Y. Abghoui, E. Skúlason, *Catal. Today* **2017**, *286*, 78.
- [62] Y. Abghoui, E. Skúlason, *J. Phys. Chem. C* **2017**, *121*, 6141.
- [63] Q. Li, L. He, C. Sun, X. Zhang, *J. Phys. Chem. C* **2017**, *121*, 27563.
- [64] L. M. Azofra, N. Li, D. R. MacFarlane, C. Sun, *Energy Environ. Sci.* **2016**, *9*, 2545.
- [65] S. Liang, C. Hao, Y. Shi, *ChemCatChem* **2015**, *7*, 2559.
- [66] C. Zhu, S. Fu, Q. Shi, D. Du, Y. Lin, *Angew. Chem., Int. Ed.* **2017**, *56*, 13944.
- [67] Y.-Q. Le, J. Gu, W. Q. Tian, *Chem. Commun.* **2014**, *50*, 13319.
- [68] X.-F. Li, Q.-K. Li, J. Cheng, L. Liu, Q. Yan, Y. Wu, X.-H. Zhang, Z.-Y. Wang, Q. Qiu, Y. Luo, *J. Am. Chem. Soc.* **2016**, *138*, 8706.
- [69] J. Zhao, Z. Chen, *J. Am. Chem. Soc.* **2017**, *139*, 12480.
- [70] L. M. Azofra, C. Sun, L. Cavallo, D. R. MacFarlane, *Chem. - Eur. J.* **2017**, *23*, 8275.
- [71] E. E. Van Tamelen, B. Akerman, *J. Am. Chem. Soc.* **1968**, *90*, 4492.
- [72] E. E. Van Tamelen, D. A. Seeley, *J. Am. Chem. Soc.* **1969**, *91*, 5194.
- [73] A. Sclafani, V. Augugliaro, M. Schiavello, *J. Electrochem. Soc.* **1983**, *130*, 734.
- [74] N. Furuya, H. Yoshioka, *J. Electroanal. Chem. Interfacial Electrochem.* **1989**, *263*, 171.
- [75] N. Furuya, H. Yoshioka, *J. Electroanal. Chem. Interfacial Electrochem.* **1990**, *291*, 269.
- [76] I. Garagounis, V. Kyriakou, A. Skodra, E. Vasileiou, M. Stoukides, *Front. Energy Res.* **2014**, *2*, 1.
- [77] G. Xu, R. Liu, J. Wang, *Sci. China, Ser. B: Chem., Life Sci., Earth Sci.* **2009**, *52*, 1171.
- [78] R. Liu, G. Xu, *Chin. J. Chem.* **2010**, *28*, 139.

- [79] R. Lan, J. T. S. Irvine, S. Tao, *Sci. Rep.* **2013**, *3*, 1145.
- [80] R. Lan, S. Tao, *RSC Advances* **2013**, *3*, 18016.
- [81] J. N. Renner, L. F. Greenlee, K. E. Ayres, A. M. Herring, *Electrochem. Soc. Interface* **2015**, *24*, 51.
- [82] J. Kong, A. Lim, C. Yoon, J. H. Jang, H. C. Ham, J. Han, S. Nam, D. Kim, Y.-E. Sung, J. Choi, H. S. Park, *ACS Sustainable Chem. Eng.* **2017**, *5*, 10986.
- [83] V. Kordali, G. Kyriacou, C. Lambrou, *Chem. Commun.* **2000**, 1673.
- [84] S. Chen, S. Perathoner, C. Ampelli, C. Mebrahtu, D. Su, G. Centi, *Angew. Chem., Int. Ed.* **2017**, *56*, 2699.
- [85] S. Chen, S. Perathoner, C. Ampelli, C. Mebrahtu, D. Su, G. Centi, *ACS Sustainable Chem. Eng.* **2017**, *5*, 7393.
- [86] G.-F. Chen, X. Cao, S. Wu, X. Zeng, L.-X. Ding, M. Zhu, H. Wang, *J. Am. Chem. Soc.* **2017**, *139*, 9771.
- [87] H.-M. Liu, S.-H. Han, Y. Zhao, Y.-Y. Zhu, X.-L. Tian, J.-H. Zeng, J.-X. Jiang, B.-Y. Xia, Y. Chen, *J. Mater. Chem. A* **2018**, *6*, 3211.
- [88] F. Köleli, T. Röpke, *Appl. Catal. B* **2006**, *62*, 306.
- [89] F. Köleli, D. B. Kayan, *J. Electroanal. Chem.* **2010**, *638*, 119.
- [90] K. Kugler, M. Luhn, J. A. Schramm, K. Rahimi, M. Wessling, *Phys. Chem. Chem. Phys.* **2015**, *17*, 3768.
- [91] K. Kim, N. Lee, C.-Y. Yoo, J.-N. Kim, H. C. Yoon, J.-I. Han, *J. Electrochem. Soc.* **2016**, *163*, F610.
- [92] K. Kim, C.-Y. Yoo, J.-N. Kim, H. C. Yoon, J.-I. Han, *J. Electrochem. Soc.* **2016**, *163*, F1523.
- [93] D. Yang, T. Chen, Z. Wang, *J. Mater. Chem. A* **2017**, *5*, 18967.
- [94] C. Lv, C. Yan, G. Chen, Y. Ding, J. Sun, Y. Zhou, G. Yu, *Angew. Chem., Int. Ed.* **2018**, <https://doi.org/10.1002/anie.201801538>.
- [95] Y. Liu, Y. Su, X. Quan, X. Fan, S. Chen, H. Yu, H. Zhao, Y. Zhang, J. Zhao, *ACS Catal.* **2018**, *8*, 1186.
- [96] H. Hirakawa, M. Hashimoto, Y. Shiraishi, T. Hirai, *J. Am. Chem. Soc.* **2017**, *139*, 10929.
- [97] C. D. Zeinalipour-Yazdi, J. S. J. Hargreaves, C. R. A. Catlow, *J. Phys. Chem. C* **2018**, *122*, 6078.
- [98] J. R. Petrie, V. R. Cooper, J. W. Freeland, T. L. Meyer, Z. Zhang, D. A. Lutterman, H. N. Lee, *J. Am. Chem. Soc.* **2016**, *138*, 2488.
- [99] T. Ling, D.-Y. Yan, H. Wang, Y. Jiao, Z. Hu, Y. Zheng, L. Zheng, J. Mao, H. Liu, X.-W. Du, M. Jaroniec, S.-Z. Qiao, *Nat. Commun.* **2017**, *8*, 1509.
- [100] Y. Xiong, H. Shan, Z. Zhou, Y. Yan, W. Chen, Y. Yang, Y. Liu, H. Tian, J. Wu, H. Zhang, D. Yang, *Small* **2017**, *13*, 1603423.
- [101] Q. Feng, S. Zhao, D. He, S. Tian, L. Gu, X. Wen, C. Chen, Q. Peng, D. Wang, Y. Li, *J. Am. Chem. Soc.* **2018**, *140*, 2773.
- [102] Y. Zhao, Y. Zhao, G. I. N. Waterhouse, L. Zheng, X. Cao, F. Teng, L.-Z. Wu, C.-H. Tung, D. O'Hare, T. Zhang, *Adv. Mater.* **2017**, *29*, 1703828.
- [103] H.-F. Wang, C. Tang, B.-Q. Li, Q. Zhang, *Inorg. Chem. Front.* **2018**, *5*, 521.
- [104] B.-Q. Li, S.-Y. Zhang, C. Tang, X. Cui, Q. Zhang, *Small* **2017**, *13*, 1700610.
- [105] J. Lai, S. Guo, *Small* **2017**, *13*, 1702156.
- [106] X. Zhang, X. Cheng, Q. Zhang, *J. Energy Chem.* **2016**, *25*, 967.
- [107] C. Tang, H.-F. Wang, X. Chen, B.-Q. Li, T.-Z. Hou, B. Zhang, Q. Zhang, M.-M. Titirici, F. Wei, *Adv. Mater.* **2016**, *28*, 6845.
- [108] C. Tang, Q. Zhang, *Adv. Mater.* **2017**, *29*, 1604103.
- [109] C. Tang, M.-M. Titirici, Q. Zhang, *J. Energy Chem.* **2017**, *26*, 1077.
- [110] L. Bu, N. Zhang, S. Guo, X. Zhang, J. Li, J. Yao, T. Wu, G. Lu, J.-Y. Ma, D. Su, X. Huang, *Science* **2016**, *354*, 1410.
- [111] H. F. Wang, C. Tang, B. Wang, B. Q. Li, Q. Zhang, *Adv. Mater.* **2017**, *29*, 1702327.
- [112] B.-Q. Li, Z.-J. Xia, B. Zhang, C. Tang, H.-F. Wang, Q. Zhang, *Nat. Commun.* **2017**, *8*, 934.
- [113] Z.-F. Huang, J. Wang, Y. Peng, C.-Y. Jung, A. Fisher, X. Wang, *Adv. Energy Mater.* **2017**, *7*, 1700544.
- [114] X. Zhao, F. Yin, N. Liu, G. Li, T. Fan, B. Chen, *J. Mater. Sci.* **2017**, *52*, 10175.
- [115] S. Lin, C. S. Diercks, Y.-B. Zhang, N. Kornienko, E. M. Nichols, Y. Zhao, A. R. Paris, D. Kim, P. Yang, O. M. Yaghi, C. J. Chang, *Science* **2015**, *349*, 1208.
- [116] N. Huang, P. Wang, D. Jiang, *Nat. Rev. Mater.* **2016**, *1*, 16068.
- [117] Y. Li, Q. Sun, *Adv. Energy Mater.* **2016**, *6*, 1600463.
- [118] H.-K. Lim, H. Shin, W. A. Goddard, Y. J. Hwang, B. K. Min, H. Kim, *J. Am. Chem. Soc.* **2014**, *136*, 11355.
- [119] B. L. Sheets, G. G. Botte, *Chem. Commun.* **2018**, *54*, 4250.
- [120] F. Zhou, L. M. Azofra, M. Ali, M. Kar, A. N. Simonov, C. McDonnell-Worth, C. Sun, X. Zhang, D. R. MacFarlane, *Energy Environ. Sci.* **2017**, *10*, 2516.
- [121] A. K. Manohar, S. Malkhandi, B. Yang, C. Yang, G. K. Surya Prakash, S. R. Narayanan, *J. Electrochem. Soc.* **2012**, *159*, A1209.
- [122] M. Chamoun, B. Skárman, H. Vidarsson, R. I. Smith, S. Hull, M. Lelis, D. Milcius, D. Noréus, *J. Electrochem. Soc.* **2017**, *164*, A1251.
- [123] S. Malkhandi, B. Yang, A. K. Manohar, G. K. S. Prakash, S. R. Narayanan, *J. Am. Chem. Soc.* **2013**, *135*, 347.
- [124] K. A. Brown, D. F. Harris, M. B. Wilker, A. Rasmussen, N. Khadka, H. Hamby, S. Keable, G. Dukovic, J. W. Peters, L. C. Seefeldt, P. W. King, *Science* **2016**, *352*, 448.
- [125] D. Zhu, L. Zhang, R. E. Ruther, R. J. Hamers, *Nat. Mater.* **2013**, *12*, 836.
- [126] T. Akira, K. Akihiko, S. Tadayoshi, *Chem. Lett.* **1993**, *22*, 851.
- [127] A. Tsuneto, A. Kudo, T. Sakata, *J. Electroanal. Chem.* **1994**, *367*, 183.
- [128] T. M. Pappenfus, K.-m. Lee, L. M. Thoma, C. R. Dukart, *ECS Trans.* **2009**, *16*, 89.
- [129] J.-L. Ma, D. Bao, M.-M. Shi, J.-M. Yan, X.-B. Zhang, *Chem* **2017**, *2*, 525.
- [130] J. M. McEnaney, A. R. Singh, J. A. Schwalbe, J. Kibsgaard, J. Lin, M. Cargnello, T. Jaramillo, J. K. Norskov, *Energy Environ. Sci.* **2017**, *10*, 1621.
- [131] K. Kim, S. J. Lee, D.-Y. Kim, C.-Y. Yoo, J. W. Choi, J.-N. Kim, Y. Woo, H. C. Yoon, J.-I. Han, *ChemSusChem* **2018**, *11*, 120.
- [132] A. Jain, H. Miyaoka, S. Kumar, T. Ichikawa, Y. Kojima, *Int. J. Hydrogen Energy* **2017**, *42*, 24897.
- [133] D. H. Thomas, M. Rey, P. E. Jackson, *J. Chromatogr. A* **2002**, *956*, 181.
- [134] R. Michalski, *Crit. Rev. Anal. Chem.* **2009**, *39*, 230.
- [135] L. Zhou, C. E. Boyd, *Aquaculture* **2016**, *450*, 187.
- [136] I. Ivančič, D. Degobbis, *Water Res.* **1984**, *18*, 1143.
- [137] V. Fourmond, C. Léger, *Angew. Chem., Int. Ed.* **2017**, *56*, 4388.
- [138] N. Amornthammarong, J.-Z. Zhang, *Anal. Chem.* **2008**, *80*, 1019.
- [139] P. E. Jackson, *Encyclopedia of Analytical Chemistry*, John Wiley & Sons, Ltd, New York, NY **2006**.
- [140] R. Michalski, I. Kurzyca, *Pol. J. Environ. Stud.* **2006**, *15*, 5.
- [141] M. C. Bruzzoniti, R. M. De Carlo, M. Fungi, *J. Sep. Sci.* **2008**, *31*, 3182.
- [142] E. W. Rice, R. B. Baird, A. D. Eaton, L. S. Clesceri, in *Standard Methods for the Examination of Water and Wastewater* (Eds: E. W. Rice, L. Bridgewater), 22nd ed., American Public Health Association, American Water Works Association, Water Environment Federation, Washington, DC **2012**, p. 4.
- [143] C. E. Bower, T. Holm-Hansen, *Can. J. Fish. Aquat. Sci.* **1980**, *37*, 794.
- [144] A. LeDuy, R. Samson, *Biotechnol. Lett.* **1982**, *4*, 303.
- [145] T. Suzuki, T. Yasuda, T. Yamané, S. Shimizu, *J. Ferment. Technol.* **1986**, *64*, 63.
- [146] N. Amornthammarong, J.-Z. Zhang, P. B. Ortner, *Anal. Methods* **2011**, *3*, 1501.
- [147] Y. Zhu, D. Yuan, H. Lin, T. Zhou, *Anal. Lett.* **2016**, *49*, 665.
- [148] Y. Zhu, D. Yuan, Y. Huang, J. Ma, S. Feng, *Anal. Chim. Acta* **2013**, *794*, 47.
- [149] Y. Zhu, D. Yuan, Y. Huang, J. Ma, S. Feng, K. Lin, *Mar. Chem.* **2014**, *162*, 114.

- [150] Y. Gong, J. Wu, M. Kitano, J. Wang, T.-N. Ye, J. Li, Y. Kobayashi, K. Kishida, H. Abe, Y. Niwa, H. Yang, T. Tada, H. Hosono, *Nat. Catal.* **2018**, *1*, 178.
- [151] L. Zhang, S. Mallikarjun Sharada, A. R. Singh, B. A. Rohr, Y. Su, L. Qiao, J. K. Norskov, *Phys. Chem. Chem. Phys.* **2018**, *20*, 4982.
- [152] B. Lassalle-Kaiser, S. Gul, J. Kern, V. K. Yachandra, J. Yano, *J. Electron. Spectrosc. Relat. Phenom.* **2017**, *221*, 18.
- [153] Y. Gorlin, B. Lassalle-Kaiser, J. D. Benck, S. Gul, S. M. Webb, V. K. Yachandra, J. Yano, T. F. Jaramillo, *J. Am. Chem. Soc.* **2013**, *135*, 8525.
- [154] S. Zhu, B. Jiang, W.-B. Cai, M. Shao, *J. Am. Chem. Soc.* **2017**, *139*, 15664.
- [155] Y. Yao, S. Zhu, H. Wang, H. Li, M. Shao, *J. Am. Chem. Soc.* **2018**, *140*, 1496.